Article

Cell Reports

Pulsatile MEK Inhibition Improves Anti-tumor Immunity and T Cell Function in Murine Kras Mutant Lung Cancer

Graphical Abstract

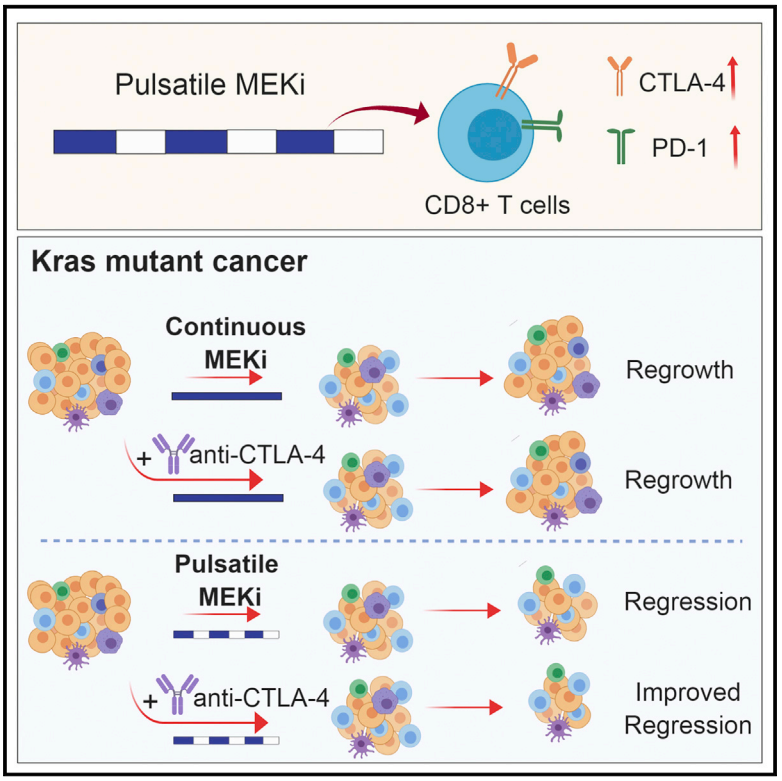

Highlights

- Pulsatile treatment with MEK inhibitors maintains T cell activation
- Pulsatile dosing of MEK inhibitor delays growth rebound of KRAS mutant lung tumors
- Combining CTLA-4 blockade with pulsatile MEK inhibition extends survival
- The enhanced survival was conferred by adaptive immunity

Authors

Hyejin Choi, Jiehui Deng, Shuai Li, ..., Taha Merghoub, Kwok-Kin Wong, Jedd D. Wolchok

Correspondence

merghout@mskcc.org (T.M.), kwok-kin.wong@nyumc.org (K.-K.W.), wolchokj@mskcc.org (J.D.W.)

In Brief

KRAS mutant non-small-cell lung cancer (NSCLC) remains refractory to targeted therapeutics. Choi et al. show that pulsatile, rather than continuous, treatment with MEK inhibitors can maintain T cell activity better and prolong survival in mice with Kras mutant cancer. This effect is further enhanced when combined with CTLA-4 blockade.

Data Resources

GSE12620

Choi et al., 2019, Cell Reports 27, 806–819
April 16, 2019
https://doi.org/10.1016/j.celrep.2019.03.066

CellPress

OPEN ACCESS
CellPress

Cell Reports
Article

Pulsatile MEK Inhibition Improves Anti-tumor Immunity and T Cell Function in Murine Kras Mutant Lung Cancer

Hyejin Choi,[1,10] Jiehui Deng,[3,10] Shuai Li,[3,10] Tarik Silk,[1] Lauren Dong,[1] Elliott J. Brea,[4,9] Sean Houghton,[1] David Redmond,[1] Hong Zhong,[1] Jonathan Boiarsky,[1] Esra A. Akbay,[5,6] Paul D. Smith,[7] Taha Merghoub,[1,2,8,9,11,*] Kwok-Kin Wong,[3,*] and Jedd D. Wolchok[1,2,8,9,*]

[1]Ludwig Collaborative and Swim Across America Laboratory, Memorial Sloan Kettering Cancer Center, New York, NY 10065, USA
[2]Parker Institute for Cancer Immunotherapy, Memorial Sloan Kettering Cancer Center, New York, NY 10065, USA
[3]Division of Hematology & Medical Oncology, Laura and Isaac Perlmutter Cancer Center, New York University Langone Medical Center, New York, NY 10016, USA
[4]Molecular Pharmacology and Chemistry Program, Sloan Kettering Institute, New York, NY 10065, USA
[5]Department of Pathology, University of Texas Southwestern Medical Center at Dallas, Dallas, TX 75390, USA
[6]Simmons Comprehensive Cancer Center, Dallas, TX 75390, USA
[7]Bioscience, iMed Oncology, AstraZeneca, CRUK Cambridge Institute, Cambridge CB2 0RE, UK
[8]Department of Medicine, Memorial Sloan Kettering Cancer Center, New York, NY 10065, USA
[9]Weill Cornell Medicine, New York, NY 10065, USA
[10]These authors contributed equally
[11]Lead Contact
*Correspondence: merghout@mskcc.org (T.M.), kwok-kin.wong@nyumc.org (K.-K.W.), wolchokj@mskcc.org (J.D.W.)
https://doi.org/10.1016/j.celrep.2019.03.066

SUMMARY

KRAS **is one of the driver oncogenes in non-small-cell lung cancer (NSCLC) but remains refractory to current modalities of targeted pathway inhibition, which include inhibiting downstream kinase MEK to circumvent KRAS activation. Here, we show that pulsatile, rather than continuous, treatment with MEK inhibitors (MEKis) maintains T cell activation and enables their proliferation. Two MEKis, selumetinib and trametinib, induce T cell activation with increased CTLA-4 expression and, to a lesser extent, PD-1 expression on T cells *in vivo* after cyclical pulsatile MEKi treatment. In addition, the pulsatile dosing schedule alone shows superior anti-tumor effects and delays the emergence of drug resistance. Furthermore, pulsatile MEKi treatment combined with CTLA-4 blockade prolongs survival in mice bearing tumors with mutant Kras. Our results set the foundation and show the importance of a combinatorial therapeutic strategy using pulsatile targeted therapy together with immunotherapy to optimally enhance tumor delay and promote long-term anti-tumor immunity.**

INTRODUCTION

The RAS-MEK-ERK signaling pathway is hyper-activated in a variety of different cancers, including non-small-cell lung cancer (NSCLC) (Fernández-Medarde and Santos, 2011). Activating mutations of KRAS are common oncogenic drivers, responsible for 20%–30% of lung adenocarcinoma patients (Lovly and Carbone, 2011). However, currently, there are no approved targeted therapies specifically for NSCLC patients with a KRAS mutation. Targeted MEK inhibitors (MEKis), which act downstream of the RAS signaling pathway, are designed to block the hyperactive signaling cascade in KRAS mutant lung cancer patients (Ostrem et al., 2013; Zeng et al., 2017) and block the proliferation and survival program in cancer cells (Riely et al., 2009).

MEKis are in diverse phases of clinical development, including trametinib, which has been approved in combination with the BRAF inhibitor dabrafenib for the treatment of a subset of NSCLC with $BRAF^{V600E}$ mutation (Friday and Adjei, 2008; Greystoke et al., 2017; Planchard et al., 2017; Stinchcombe and Johnson, 2014). However, despite promising co-clinical studies in mouse models and clinical trials (Chen et al., 2012; Greystoke et al., 2017; Planchard et al., 2017), resistance to MEKis is often observed (Soria et al., 2017). This resistance has been attributed to the heterogeneity of the tumor (Jamal-Hanjani et al., 2017; Swanton and Govindan, 2016) and to intrinsic and acquired resistance from both cancer cells and the tumor microenvironment (Ebert et al., 2016; Manchado et al., 2016). Therefore, there is a need to further improve the efficacy of MEKis in KRAS-driven lung cancer. A theoretically promising therapeutic approach would entail simultaneously blocking KRAS signaling and activating tumor-infiltrating T cells, the latter being relevant given the recent demonstration of activity of immune checkpoint blockade of the CTLA-4 and PD-1 pathways in NSCLC and other malignancies (Borghaei et al., 2015; Brahmer et al., 2015; Garon et al., 2015; Reck et al., 2016; Wolchok et al., 2013). Despite the success of immune-based therapies, the need remains for better treatment strategies for the majority of patients with advanced NSCLC, since the response to current single-agent PD-1 pathway blockade is durable only in a subset of patients (Borghaei et al., 2015; Brahmer et al., 2015), and initial results in

combination with CTLA-4 blockade showed promising efficacy for the treatment of NSCLC only in a subset of patients (Hellmann et al., 2017).

Based on the limitations of both immune-based therapies and targeted therapies, we sought to rationally combine these two modalities to treat KRAS mutant lung cancers. In addition to the essential role of MEKis in RAS-MEK-ERK signaling suppression during the tumorigenesis of NSCLC, the effect of MEKis on immune cells is complex and context dependent. The RAS-MEK-ERK signaling cascade is critical in the normal physiologic function of immune cells, especially T cells (Weiss and Littman, 1994). The sequential signaling of RAS-MEK-ERK after T cell receptor (TCR) activation is responsible for the activity of NFAT and the production of interleukin (IL)-2, which are critical for T cell clonal expansion (Kane et al., 2000; Weiss and Littman, 1994). Previous studies have shown that inhibition of MEK signaling by small molecules reduces or regulates paradoxically the proliferation of T cells *in vitro* (Callahan et al., 2014; Liu et al., 2015a). Nevertheless, it enhances the proliferation of tumor-infiltrating CD8+ T cells in CT26 Kras mutant colorectal cancer, resulting in the expansion of tumor-reactive T cell populations with cytotoxic activity (Ebert et al., 2016; Liu et al., 2015a). However, conventional continuous administration of MEKis achieves an inadequate inhibition of ERK activity, which induces feedback regulation of other proliferation and survival pathways and re-activates MEK-ERK signaling, leading to drug resistance (Samatar and Poulikakos, 2014; Sun et al., 2014). Moreover, prolonged blockade of TCR signaling by MEKis interferes with effector function and proliferation at the tumor site (Dushyanthen et al., 2017). The recent failure of a clinical trial with continuous MEKi (cobimetinib) and anti-PD-L1 (atozolizumab) combination treatment in colorectal cancer (phase III IMblaze370 study, NCT02788279) suggests that the scheduling of these drugs needs optimization.

Unconventional pulsatile treatment schedules using targeted drugs such as the BRAF inhibitor vemurafenib and the EGFR inhibitor gefitinib showed better suppression of tumor growth in melanoma, breast cancer, and leukemia (Das Thakur et al., 2013; Shah et al., 2008; Solit et al., 2005). In support of this pulsatile treatment regimen in the case of MEKis, transient pretreatment or lead-in treatment with MEKis in combination with anti-CTLA-4 or anti-PD-1 showed better survival and lower tumor burden in the CT26 mouse tumor model (Poon et al., 2017). Despite these encouraging observations, the status of T cell activation using these unconventional regimens has not been explored systematically. We hypothesize that through an optimized MEKi dosing schedule, we can maximize the suppression of KRAS-induced proliferation and survival of cancer cells while minimizing the detrimental effects on immune cells.

In this study, we have investigated how a pulsatile dosing schedule of MEKis affects T cell activation in mutant KRAS-driven lung cancer models both *ex vivo* and *in vivo*. We observed that pulsatile treatment induced improved proliferation and activation of T cells with higher expression levels of immune checkpoint regulators, including CTLA-4 and PD-1, when compared with the conventional continuous treatment with the same drug. This optimized schedule of pulsatile treatment resulted in delayed tumor growth in KRAS mutant genetically engineered mouse models (GEMMs). Furthermore, the combination of pulsatile MEKis with CTLA-4 blockade resulted in prolonged survival of mice with KRAS mutant lung cancer compared to continuous treatment with MEKis in combination with anti-CTLA-4.

RESULTS

MEK Inhibition Affects Tumor Growth in Kras Mutant Lung Cancer and MAPK Signaling in Both Tumor Cells and T Cells

We have treated various *Kras* mutant murine lung cancer cell lines (CL13, CL25, IO33, HKP1, and LLC) with selumetinib or trametinib to examine whether they are sensitive to clinically relevant MEKis. The HKP1 cell line was derived from a *Kras*$^{G12D/+}$ *Trp53*$^{-/-}$ mouse (Choi et al., 2015). We characterized the mutations in the IO33, CL13, CL25 and LLC cell lines and identified G12V, Q61R, Q61H, and G12C Kras mutations, respectively (Figure S1A). We observed that MEKis block phosphorylation of ERK in *Kras* mutant cells effectively (Figure 1A) and that tumor cells show reduced viability after treatment (Figure 1B). Furthermore, selumetinib extends the survival of HKP1 lung tumor-bearing mice, suggesting cytotoxic activity on *Kras* mutant lung cancer *in vivo* (Figure 1C). When we characterized T cells, we found decreased viability and reduced pERK in CD8+ T cells and CD4+ T cells (Figures 1D and S1B). We also observed increased interferon (IFN)γ expression in lung-infiltrating CD8+ T cells, but not in CD4+ T cells after *in vivo* selumetinib treatment (Figure S1C), which suggests differential regulation by MEKis in distinct immune cell populations. Taken together, these data confirm that MEKis can dampen signaling in the ERK pathway in both tumor cells and T cells and that combining MEKis with immune modulation should be done carefully with respect to timing.

Short (Pulsatile), but Not Long (Continuous), Treatment with MEKis Activates T Cells *Ex Vivo*

To investigate how short treatment with MEKis affect T cell activation, we treated splenocytes from HKP1 lung tumor-bearing mice *in vitro* with selumetinib or trametinib in a long or short schedule while activating T cells using anti-CD3 and anti-CD28 (Figure 2A; Figure S2). Treatment with selumetinib or trametinib reduced expression of Ki-67, 4-1BB, CTLA-4, and PD-1 from T cells in a dose-dependent manner (Figure 2B). However, short schedule treatment maintained them (Ki-67, 4-1BB, CTLA-4, and PD-1) better in CD8+ T cells and CD4+Foxp3− effector T cells, compared to long drug exposure (Figures 2B and S2). This suggests that short treatment with MEKis maintain T cells in a more activated state than continuous treatment.

Short Treatment with MEKis Increases Effector T Cell Priming

Since it has been shown previously that a MEKi (cobimetinib) reduces priming of T cells in lymph nodes (Ebert et al., 2016), we tested how short treatment with MEKis affects priming of antigen-specific (Pmel-1) CD8+ T cells. Splenocytes from Pmel-1 TCR transgenic mice were pulsed with gp100 (Pmel) peptide and treated with selumetinib or trametinib (Figure 3A). We found

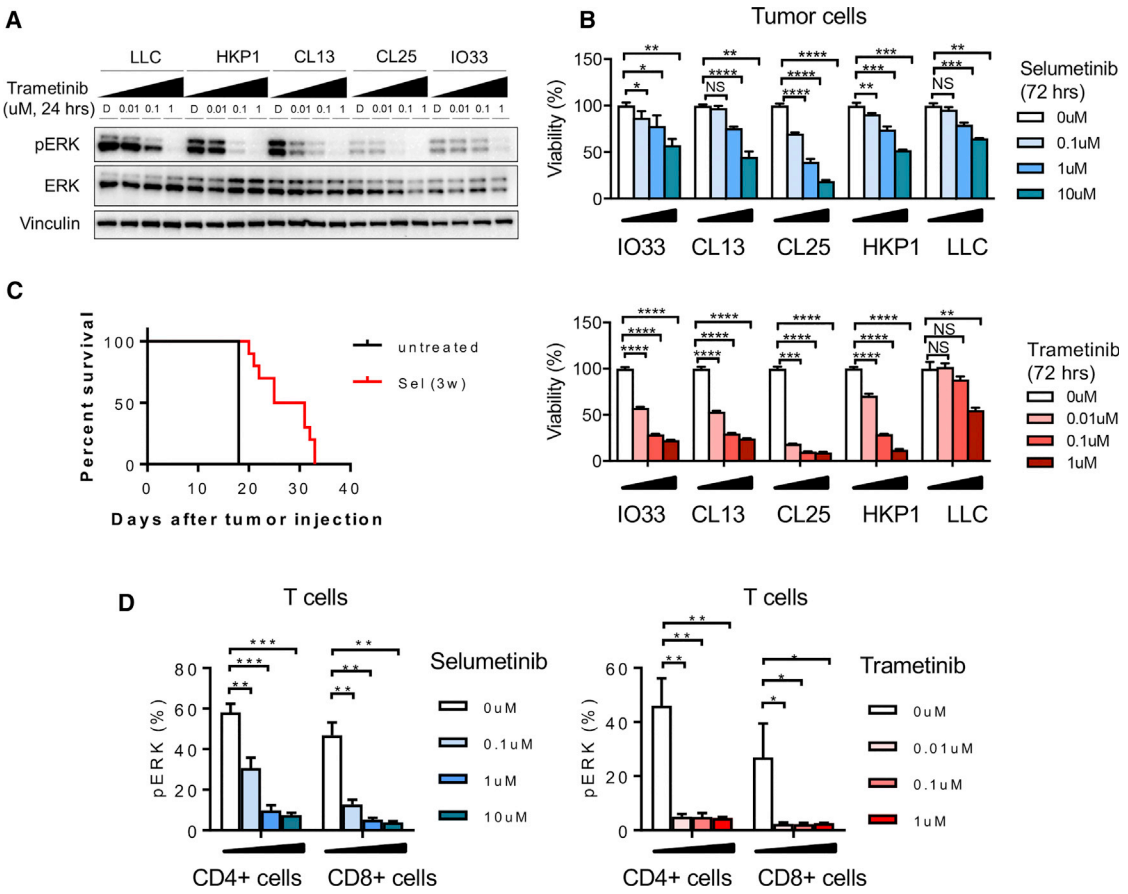

Figure 1. MEK Inhibition Affects Murine Kras Mutant Tumor Growth and Murine T Cell Signaling

(A) pERK expression in various Kras mutant lung cancer cell lines after trametinib treatment by western blot.

(B) Viability of lung tumor cell lines after selumetinib treatment. Samples were biological replicates.

(C) Survival of HKP1 lung-cancer-bearing mice after 3 weeks selumetinib treatment.

(D) pERK expression in CD4+ and CD8+ T cells from HKP1 tumor-bearing lungs after selumetinib or trametinib treatment by flow cytometry.

Samples were biological replicates. *p < 0.05; **p < 0.01; ***p < 0.001; and ****p < 0.0001, Welch's t test. NS, not significant. Error bars represent SD. The experiments were performed 2–3 times, and representative results are shown here.

that MEKi treatment reduced differentiation of Pmel-1 CD8+ T cells by decreasing T-bet expression in a dose-dependent manner (Figure S3A), as was previously reported (Ebert et al., 2016). However, we have not observed differences in T-bet expression between the two treatment groups (Figure S3A). Selumetinib and trametinib treatment resulted in increased CD44+CD62L− effector memory CD8 T cells, as well as reduced CD44+CD62L+ central memory CD8 T cells, compared to untreated samples (Figures 3B and 3C). However, short treatment with MEKis showed more CD44+ cells, specifically CD44+CD62L− CD8 T cells, compared to long treatment (Figures 3B–3D). Interestingly, CD44+CD62L+ CD8 T cells and naive cells showed decreased proliferation after selumetinib treatment in both groups, while CD44+CD62L− CD8 T cells showed a more proliferative phenotype compared to other subsets, regardless of treatment conditions (Figure S3B). Furthermore, analysis of the supernatant after priming showed that the short-treatment group had a higher production of IFNγ, suggesting better cytolytic capability (Figure 3E).

Pulsatile Treatment with MEKis Increases CTLA-4 and PD-1 Expression in Tumor-Infiltrating T Cells compared to Continuous Treatment

Next, we investigated whether cyclical pulsatile treatment with MEKis shows differential activation of different subtypes of T cells *in vivo*. We treated HKP1 lung tumor-bearing mice with selumetinib (Figure 4A). After 2 weeks of treatment, lung tumors were analyzed for the activation phenotype of tumor-infiltrating T cells. Tumors were highly infiltrated by CD8+ T cells in the pulsatile treatment groups (Figures 4B and S4C). More importantly, tumor cells and CD8+ T cells showed differential proliferation (Ki-67+) with the pulsatile treatment. While proliferation of tumor cells was reduced, CD8+ T cells showed increased or stable proliferation (Figure 4C). These observations suggest that individual T cell populations respond to MEKi treatment differently. Furthermore, pulsatile treatment with selumetinib results in the maintenance of a higher level of pERK in both CD8+ and CD4+ T cells, compared to continuous treatment (Figure S4), suggesting reduced suppression of MEK signaling pathways by pulsatile

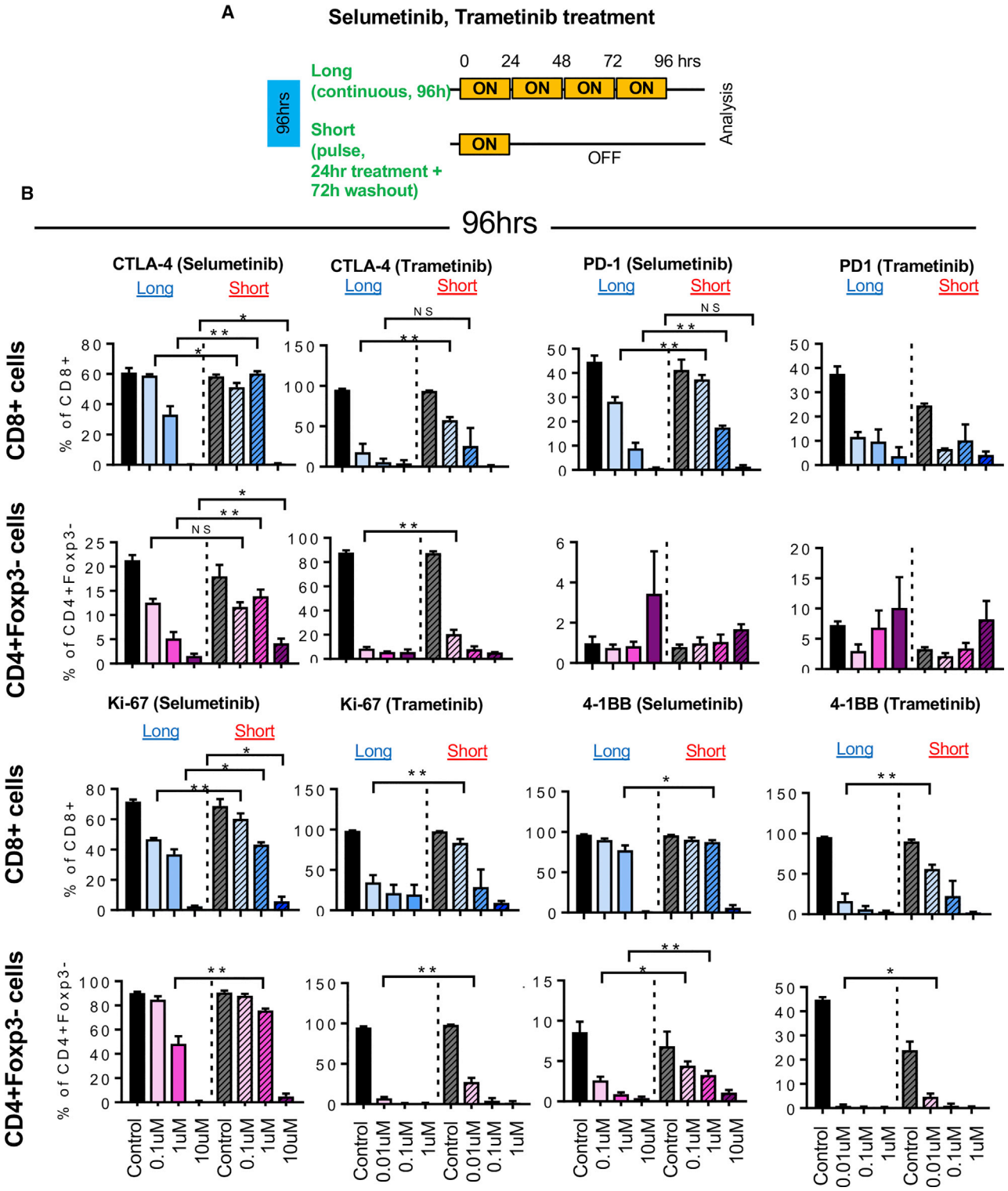

Figure 2. Short Schedule of MEKi Treatment Alters T Cell Activation Status *Ex Vivo*

(A) Schema of *ex vivo* short versus long treatment experiment.

(B) CTLA-4, PD1, Ki-67, and 4-1BB expression in CD8+ T cells and CD4+Foxp3− cells by flow cytometry after selumetinib (left) or trametinib (right) treatment for 96 hr. *$p < 0.05$; **$p < 0.01$, Welch's test.

Error bars represent SD. Samples were biological replicates. The experiment was performed twice, and representative results are shown here.

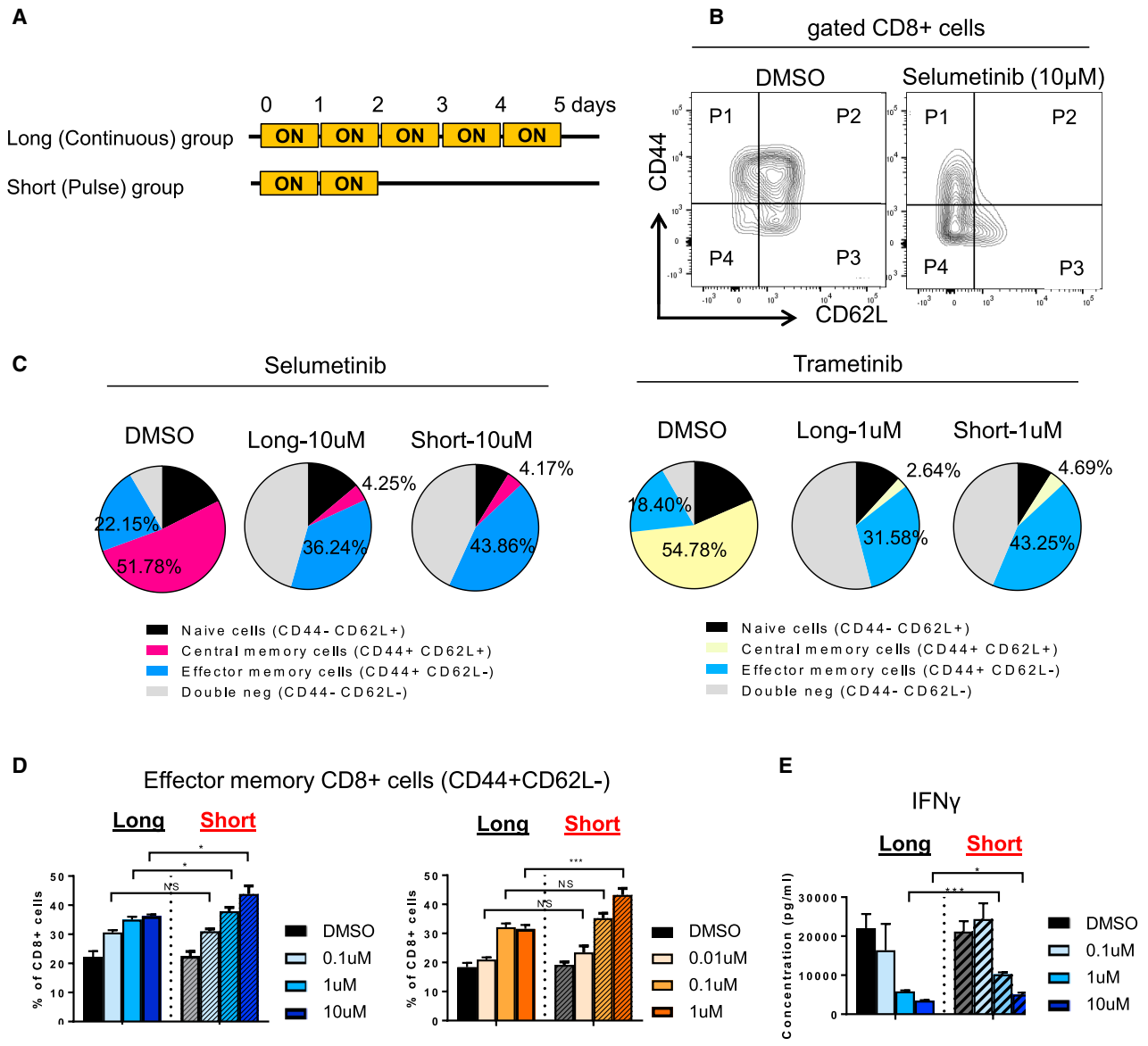

Figure 3. Short Treatment of MEKis Alters T Cell Priming *Ex Vivo*

(A) Schema of short treatment on Pmel-1 CD8+ T cells with human gp100 peptide pulse.

(B) Flow cytometry plots of CD44 and CD62L markers on CD8+ T cells after 5 days of priming.

(C) Frequency of CD44 CD62L subsets from CD8+ T cells by flow cytometry analysis. Average percentage of each subset is presented.

(D) Frequency of CD44+ CD62L− cell population by flow cytometry.

(E) IFNγ production from supernatant at day 5 by cytokine profiling.

*p < 0.05; **p < 0.01; ***p < 0.001, Welch's test. Error bars represent SD. Samples were biological replicates. The experiment was performed twice, and representative results are shown here.

treatment in T cells. Consistent with *ex vivo* observations, CTLA-4 and PD-1 expression on CD8+ T cells were significantly higher with pulsatile treatment (Figure 4D). Additionally, PD-1 showed a significant increase in CD4+ T cells (CD4+Foxp3− and CD4+Foxp3+) and only a slight increase in CD8+ T cells (Figure 4D). We have observed similar results with pulsatile MEKi treatment at higher doses and a longer lag time (Figures S4B–S4D). T-bet expression is higher with pulsatile treatment in CD4+ T cells and CD8+ T cells from lung tumors (Figure S4C). Many co-stimulatory markers were increased in the regulatory T cell (Treg cell) population, but not in CD4+ T cells or CD8+ T cells, indicating differential regulation in subsets of T cells after pulsatile treatment (Figure S4D). Collectively, these observations indicate that pulsatile treatment with MEKi may establish

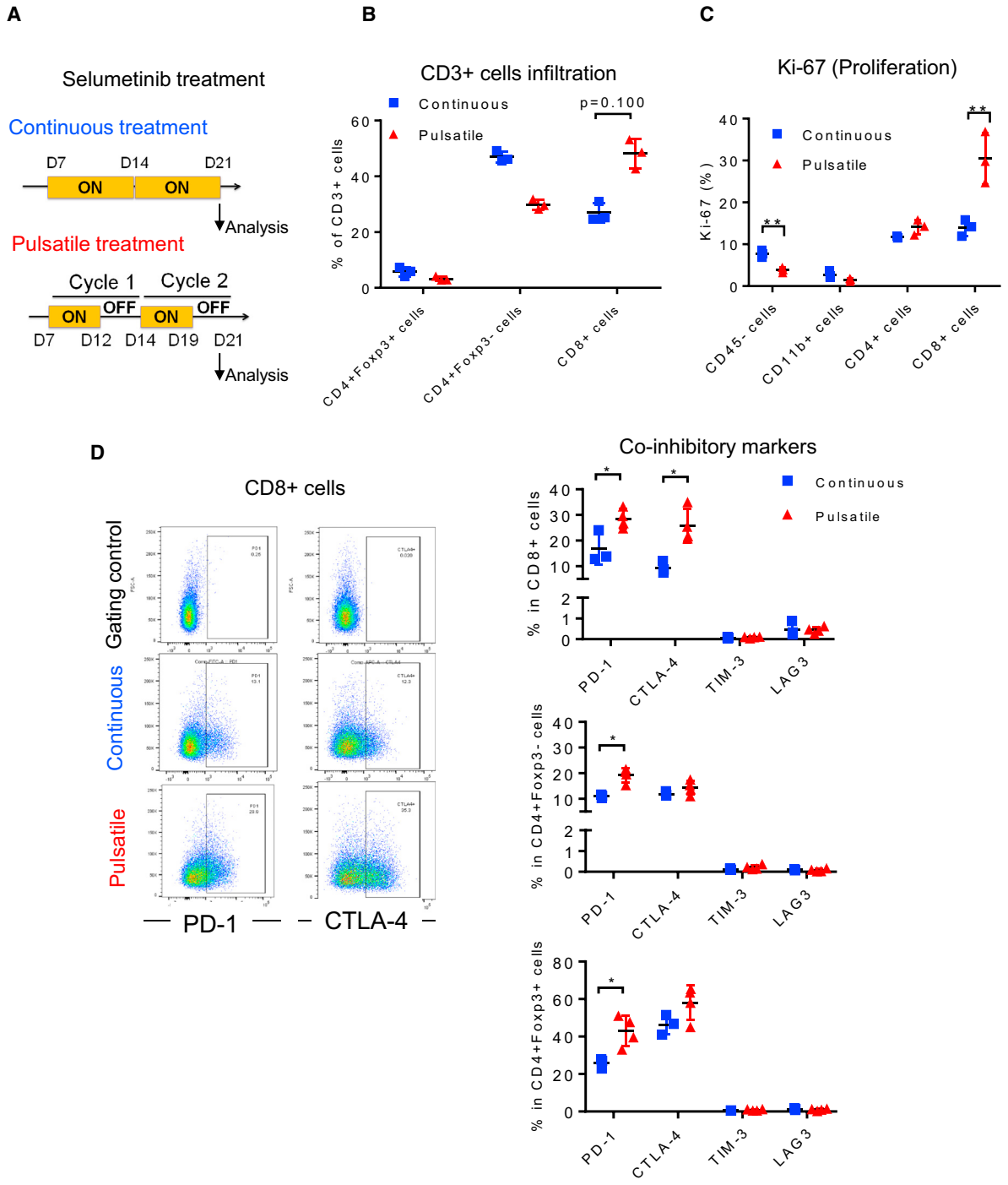

Figure 4. Pulsatile Treatment of Selumetinib Induces CTLA-4 and PD-1 Expression *In Vivo*

HKP1 transplantable lung-tumor-bearing mice were treated with selumetinib (25 mg/kg, BID) as presented in (A). After 2 weeks of treatment, lungs were collected and analyzed by flow cytometry.

(A) Schema of selumetinib treatment in HKP1 lung-tumor-bearing mice *in vivo*.

(B) Frequency of CD3+ T cell subsets in lung tumors by flow cytometry.

(C) Ki-67 of diverse cell populations in lung tumors by flow cytometry.

(D) Scatterplots of PD-1 and CTLA-4 marker (left) and co-inhibitory marker expression from CD3+ T cell subsets of lung tumors by flow cytometry (right). Gating controls are samples without either PD-1 or CTLA-4 antibodies.

*$p < 0.05$; **$p < 0.01$; ***$p < 0.001$, Mann-Whitney test. Samples were biological replicates. The experiment was performed 3 times, and representative results are shown here.

a tumor microenvironment that suppresses tumor growth while maintaining optimal CD8+ activation and infiltration in the tumor microenvironment.

Pulsatile MEKi Treatment Delays Tumor Growth *In Vivo*

We next tested whether pulsatile treatment confers better anti-tumor activity compared with continuous dosing. We used the *Kras*^{G12D} mutated HKP1 transplantable tumor model. Though there was a transient delay of tumor growth (Figure S4E), we did not observe differences in tumor progression and survival between the pulsatile and the continuous treatment groups in these settings (Figure S4F). The absence of differential effects may be due to the highly aggressive nature of these transplantable tumors.

In order to further investigate the effects of MEKi treatment regimens, we utilized the *KRAS*^{G12C} GEMM, an autochthonous model that has a slower tumor progression rate and allows for a better therapeutic window. Intranasal instillation of adenovirus with CRE recombinase expression similarly induces lung tumor formation, as the endogenous *Kras*^{G12D} lung cancer GEMM model previously reported (Chen et al., 2012). Given the similarity of the data between selumetinib and trametinib, we focused our experiments on one MEKi, selumetinib, in the GEMM experiments. After the mice developed lung tumors, a group of mice was treated continuously with selumetinib, with similar baseline tumor volumes (Figure 5A; Figures S5A and S5B). In the first week of the treatment, these mice responded to MEKi, and tumor sizes started to decrease as quantified by MRI imaging (Figure 5B). In the second week, about 50% of the mice developed resistance to treatment, and tumors regrew (Figure 5B; Figure S5B). This is consistent with prior work (Li et al., 2018) . In contrast, when we treated mice with selumetinib following a cyclical pulsatile schedule of 1 week on and 1 week off (Figure 5A), the tumors continued to respond to MEKi and had reduced tumor volume, while untreated control tumors continued to grow (Figure 5C; Figure S5B). Both the continuous and pulsatile treatment groups showed decreased levels of pERK in tumor cells compared to the control group, but the continuous group had the lowest pERK expression (Figure 5D). Supporting this pERK suppression, the MEK signaling activation gene signature (Brant et al., 2017) showed consistent suppression of the MEK signaling pathway in the majority of samples in the pulsatile and continuous groups (Figure S5C). Overall, mice treated with pulsatile selumetinib had significantly prolonged progression-free survival compared with those treated with either continuous selumetinib or vehicle control. (Figure 5E).

Pulsatile Treatment Induces Anti-tumor Immunity through T Cells

To understand the potential contribution of T cells in the observed anti-tumor effect, we analyzed the lungs from the *KRAS*^{G12C} GEMMs at the end of each treatment with selumetinib (continuous or pulsatile schedule; Figure 5A). The percentage of tumor-infiltrating T lymphocytes, including CD4+ T cells and CD8+ T cells, did not show significant differences within the total infiltrating CD45+ leukocytes (Figure 6A). The percentage of Treg cells was increased with either continuous or pulsatile selumetinib treatment. However, this was not correlated with tumor volume changes in the pulsatile or continuous dosing schedule (Figures 5B, 5C, and 6A), suggesting that Tregs may not play a major role in this setting, since these two treatment schedules gave different responses despite the increase of Tregs in both conditions. At the end of pulsatile selumetinib treatment, we observed increased levels of CTLA-4 on both CD4+ and CD8+ T cells (Figure 6D; Figure S6A). Although PD-1 levels are also slightly increased in the pulsatile treatment group, the difference between control and treated groups is not statistically significant (Figure 6D; Figure S6A). On the other hand, at the end of continuous treatment with selumetinib, PD-1 expression was decreased in both CD4+ and CD8+ T cells, while CTLA-4 was only found to be downregulated in CD8+ T cells, as determined by both percentage and median fluorescence intensity (MFI) (Figures 6B, 6C, and S6A). The expression levels of both PD-1 and CTLA-4 are high in Treg cells. After pulsatile treatment with selumetinib, the expression levels of PD-1 and CTLA-4 remained unchanged (Figure S6B). In contrast, continuous selumetinib treatment reduced CTLA-4, but not PD-1, levels on Tregs (Figure S6B). The co-inhibitory molecules LAG3 and TIM3 did not show major expression level changes in CD4+ or CD8+ T cells with either treatment schedule (Figures 6C and 6D). Additionally, pulsatile treatment with selumetinib showed a trend toward increased CD69 and Ki-67 expression, indicating that T cells are modestly more activated after pulsatile treatment (Figure S6C). Continuous selumetinib treatment was found to decrease PD-L1 expression only in CD11b+ myeloid cells and increase its expression in CD8+ T cells. Pulsatile selumetinib treatment significantly downregulated PD-L1 levels in EpCAM+, CD11b+, and CD4+ T cells (Figure S6D). Neither pulsatile nor continuous treatment affected the infiltration of CD11b+ myeloid populations significantly (Figure S6E).

Taken together, our data show that pulsatile MEKi treatment results in improved activation of tumor-infiltrating T cells. Interestingly, when we used higher doses (>10-fold) of selumetinib with a pulsatile schedule *in vivo* (Figure 7A), there was no evident detrimental effect on the immune system in terms of T cell frequency and PD-L1 expression (Figure 7B). T cells were activated 3 days after the treatment was stopped, as determined by Ki-67 and CTLA-4 expression on CD8+ T cells (Figures 7B and 7C). In addition, high-dose pulsatile treatment with selumetinib does not seem to restrain the proliferation of T cells (Figure 7B).

Combination Therapy with Pulsatile MEKis and CTLA-4 Blockade Enhances Survival in Mice with Kras Mutated Lung Tumors

Based on the aforementioned observations, we combined CTLA-4 blockade with pulsatile selumetinib treatment to investigate whether the enhanced T cell activation associated with the pulsatile schedule can produce a better outcome in combination with the checkpoint blockade in tumor-bearing mice. We chose a high concentration of selumetinib for pulsatile treatment since proliferation and CTLA-4 expression were elevated, per the previous experiments (Figures 7B and 7C), and tested in a transplantable LLC model (same Kras mutation as the GEMM). We found that the combination of pulsatile high doses of selumetinib with a 3-day gap and CTLA-4 blockade provided the longest survival in mice as compared to other monotherapies

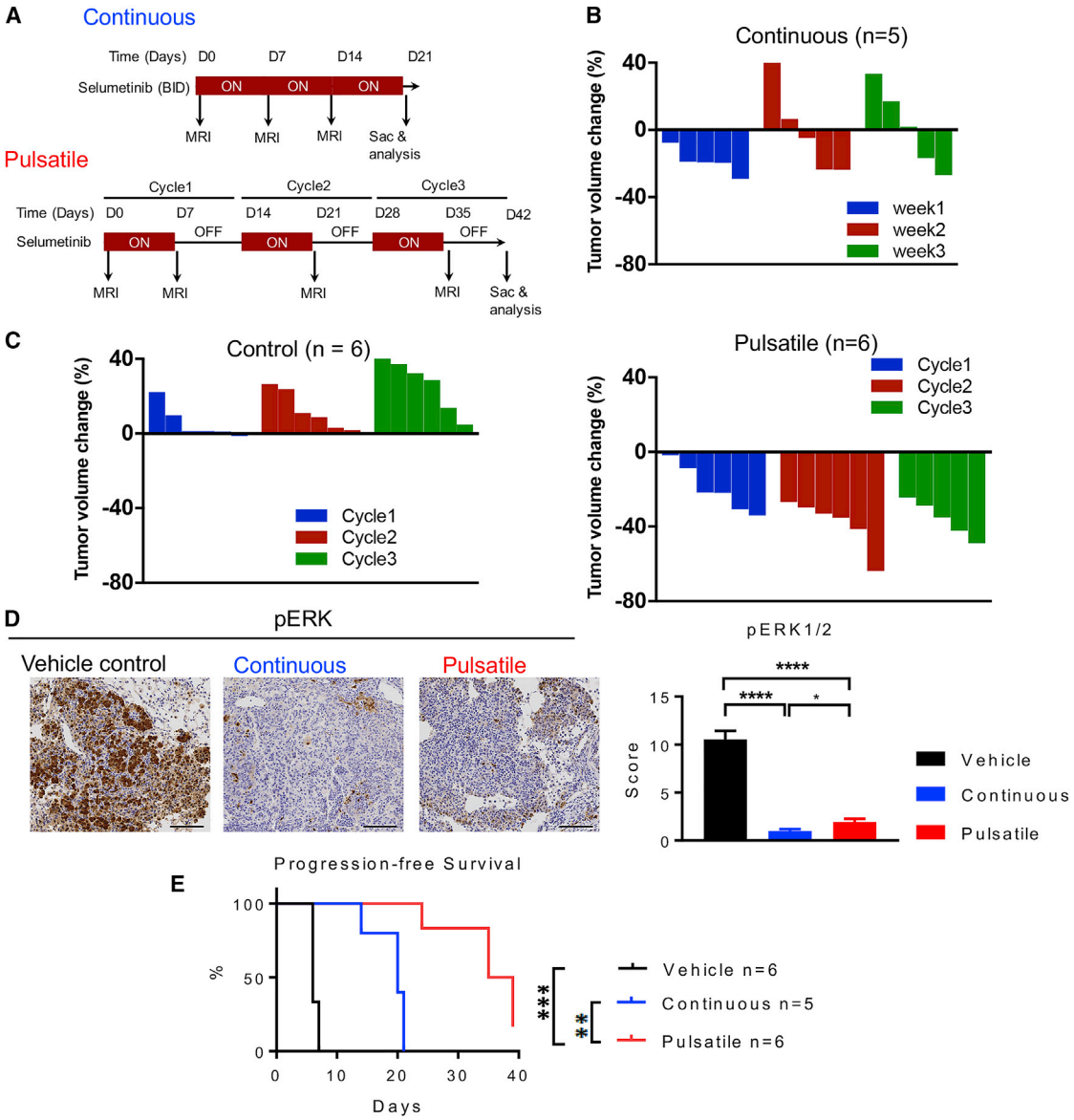

Figure 5. Pulsatile Schedule of MEKi Treatment Delays Tumor Growth *In Vivo*

(A) Schema of selumetinib treatment in *KRAS*^{G12C} mutant genetically engineered mouse model (GEMM) of lung cancer. Treatment schedule for continuous treatment (upper panel, 25 mg/kg, BID) and pulsatile treatment (lower panel, 25 mg/kg, BID).

(B) Waterfall plot showing tumor volume change at indicated time points after the continuous treatment of selumetinib.

(C) Waterfall plot showing tumor volume change at indicated time points after the treatment of pulsatile dosing of either vehicle (left panel) or selumetinib (right panel).

(D) Representative images of immunohistochemistry (IHC) staining of pERK (left panels) and multiplicative quick scores for quantification of pERK1/2 staining with vehicle control, pulsatile selumetinib, or continuous selumetinib for tumor tissue samples at the end of the treatment (right panel). Scale bars, 100 μm. *$p < 0.05$; ****$p < 0.0001$.

(E) Progression-free survival of *KRAS*^{G12C} mice treated with vehicle control, pulsatile selumetinib, or continuous selumetinib. **$p < 0.01$; ***$p < 0.001$.

Samples were biological replicates. This treatment study was performed three times, and results from all mice have been combined as presented.

or combination therapies (Figures 7D and 7E). The survival advantage was lost in Rag$^{-/-}$ mice, which are deficient in T and B cells (Figures 7F and 7G), suggesting that adaptive immunity contributes to improved survival in this treatment setting. Interestingly, MEKis combined with PD-1 targeting did not improve survival further (Figure S7A). In addition to the contribution of adaptive immune cells in MEKi treatment, we also observed a potential contribution of NK cells to survival in both MEKi treatment groups (Figures S7B and S7C). Although the survival difference in the anti-CTLA-4 combination is modest in our

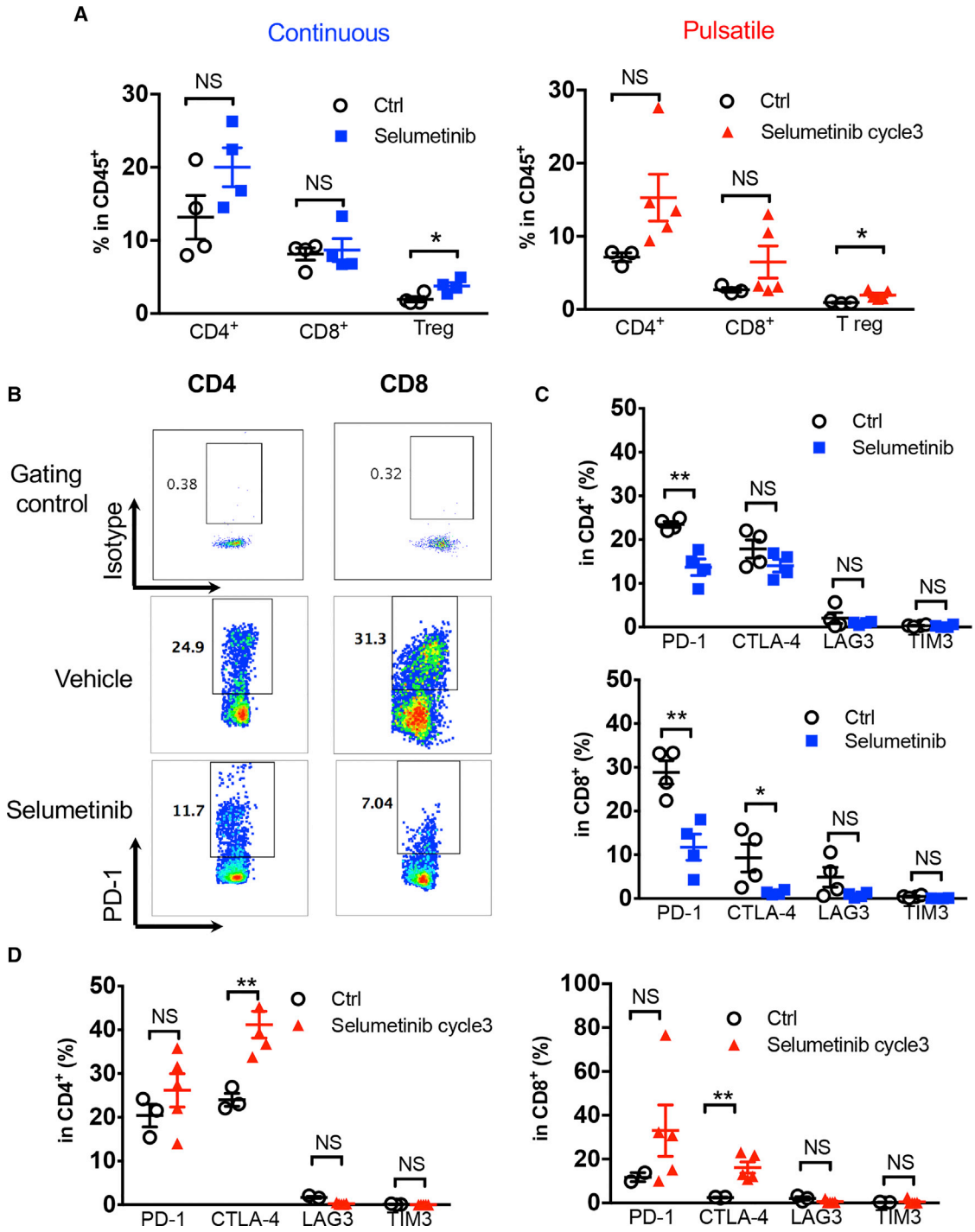

Figure 6. Co-inhibitory Signaling Was Altered Differentially by Continuous versus Pulsatile Treatment of MEKis

(A) Flow cytometry analysis of *KRAS*^{G12C} mutant GEMM lung-tumor-infiltrating T cell subpopulations: CD4+, CD8+, and Tregs (CD4+Foxp3+) after continuous (left) or pulsatile (right) treatment with selumetinib as presented in Figure 5A. Lung tumors were collected at the end of treatment. *$p < 0.05$. NS, not significant.

(B) Representative flow cytometry analysis of PD-1 levels in both CD4+ and CD8+ tumor-infiltrating T cells after continuous treatment of selumetinib.

(C) Quantification of inhibitory immune checkpoint molecule expression on CD4+ (upper) and CD8+ (lower) T cells after 3 weeks of continuous selumetinib treatment. *$p < 0.05$; **$p < 0.01$.

(D) Quantification of inhibitory molecules within CD4+ (left) and CD8+ (right) T lymphocyte subpopulations after 3 cycles of pulsatile selumetinib treatment. **$p < 0.01$.

Samples were biological replicates. All mice were recruited at the same time for the treatment, and results from all mice are shown here.

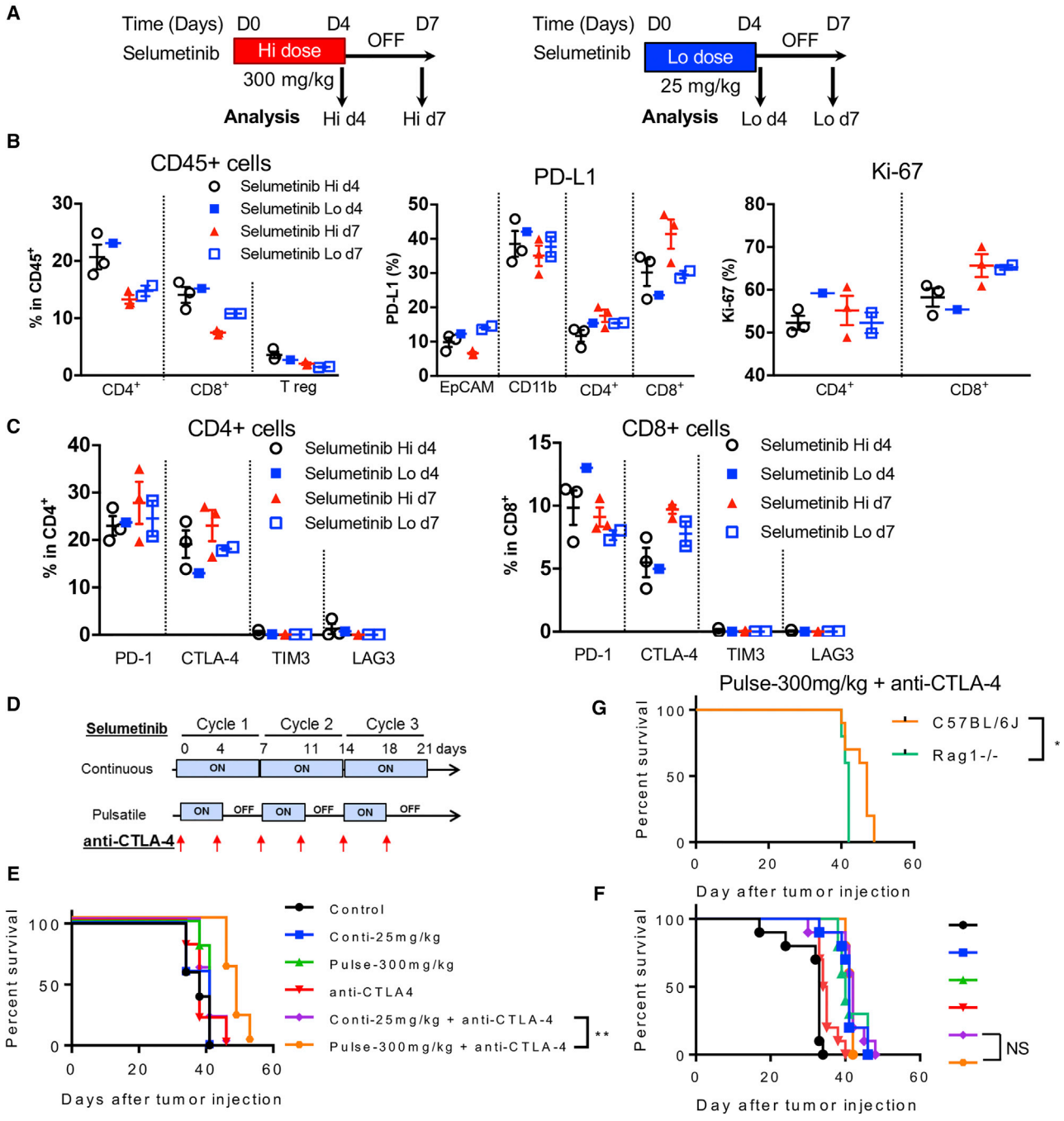

Figure 7. Pulsatile Treatment of Selumetinib with High Dosage Impacts Immune Microenvironment Differently and Enhances Survival in Combination with Anti-CTLA-4 Treatment

(A) Schema of dosing and sample collection after either high-dose (Hi; 600 mg/kg/day; left panel) or low-dose (Lo; 50 mg/kg/day; right panel) selumetinib treatment. *Kras*^{G12D}*Trp53*$^{fl/fl}$ murine transplantable tumors were treated with different dosages of selumetinib. Mouse lung tumors were collected at indicated time points. Samples were biological replicates.

(B) Flow cytometry analysis of different tumor-infiltrating T cell subpopulations within total infiltrating CD45+ leukocytes at indicated time points (left). PD-L1 expression levels on tumor cells (EpCAM+), myeloid cells (CD11b+), and T cells (CD4+ and CD8+) (middle); and Ki-67 expression (right).

(C) Quantification of inhibitory immune checkpoint molecules expressed on CD4+ (left) and CD8+ (right) T cells.

(D) Schema of selumetinib and anti-CTLA-4 treatment on LLC transplantable tumor model.

(E) Survival curve from the selumetinib and anti-CTLA-4 treatment combination in immune-competent mice (C57BL/6J).

(legend continued on next page)

experimental settings, these results bring forth the possibility that the combination of CTLA-4 blockade with pulsatile MEKi might be considered for clinical trials as a treatment strategy for KRAS mutated lung cancers.

DISCUSSION

In this study, we have demonstrated that, as opposed to conventional continuous MEKi treatment used in the clinic, a pulsatile schedule of MEKi treatment is more effective at controlling tumor progression and enhancing T cell activation with increased levels of CTLA-4 and PD-1 expression. In comparison with continuous treatment, *ex vivo* pulsatile treatment of T cells with MEKis (selumetinib or trametinib), alongside activation by anti-CD3 and anti-CD28 antibodies, resulted in increased CTLA-4 expression and, to a lesser extent, PD-1 expression. Concurrent changes of Ki-67 and 4-1BB suggest that both CD8+ T cells and CD4+Foxp3− effector cells are more activated by pulsatile treatment with MEKis. While changes in CD4+Foxp3− effector cells and CD4+Foxp3+ T cells are subtle, CD8+ T cells showed high expression levels of immune checkpoint regulators and co-stimulatory markers. This might be due to the fact that CD8+ T cells and CD4+ T cells are regulated through distinct signaling pathways with varying dependence on the mitogen-activated protein (MAP) kinase pathway. In CD8+ T cells, MEK1/2-ERK1/2 signaling is critical for cytotoxic activity, proliferation, and survival (Rincón et al., 2001; D'Souza et al., 2008). In CD4+ T cells, MEK4/6/7-p38 and JNK are more important for their activity and development (Rincón et al., 2001). This differential dependency on distinct signaling pathways may regulate responses of CD8+ T cells and CD4+ T cells to MEKis in a different fashion.

In addition to changes in T cells, MEKi increases major histocompatibility complex class I (MHC I) expression, which is essential for cytotoxic T cell activation, in tumor cells (Brea et al., 2016). In our preliminary data, we observed an increase of H2-Kb MHC I expression in the CD45− cell population after pulsatile MEK inhibition in HKP1 lung tumors. However, after a 2–3 day "washout" period, MHC I expression decreased gradually to the levels of untreated tumors (data not shown). These data further underscore the importance of timing when MEKi treatment and combination approaches are designed.

Our *in vivo* data with pulsatile MEKis in a transplantable Kras model are consistent with the *ex vivo* observations. The effects of pulsatile MEKi treatment were more pronounced on CD8+ T cells infiltrating into tumors and their expression of CTLA-4 and PD-1. *In vivo*, T cells that are being treated have not been pre-selected (as opposed to *ex vivo*, where cells come from one anatomical location); as a result, we can speculate that cells exposed to MEKis are at different stages of T cell development *in vivo*. It has been shown previously that the MEK/ERK pathway is fundamental to T cell lineage commitment in the thymus during development. Genetic reduction of ERK induces more CD8+ cells from CD4+ CD8+ double-positive T cells via loss of CD4+ markers in the thymus (Rincón et al., 2001). While pERK reduction is preferable for CD8 expansion in the thymus, pERK positively regulates CD8+ T cell proliferation, survival, and IL-2 cytokine expression from CD8+ cells (Rincón et al., 2001; D'Souza et al., 2008). Furthermore, activation of MEK/ERK signaling downregulates apoptosis in activated primary peripheral T cells (Holmström et al., 2000). Thus, we can speculate that, with pulsatile MEKis, more CD8+ cells will be generated in the thymus during the treatment, then following a period without MEKis treatment may allow proliferation or reduce apoptosis of differentiated CD8+ cells globally, resulting in an expansion of CD8+ populations in the tumor. Considering this intricate role of ERK in CD8+ T cells from development to activation and survival, ERK signaling may be best modulated using a rationally designed schedule in order to maximize the frequency and activation of CD8+ T cells. Our pulsatile schedule of treatment demonstrates better control of this signaling pathway by increasing the frequency of CD8+ T cells and their expression of activation markers and immunotherapy targets in Kras mutated lung tumors.

MEK inhibition in tumor-bearing mice has been previously reported to interfere with the priming of T cells in lymph node yet enhance CD8+ T cell expansion in a CT26 tumor site due to reduced apoptosis (Ebert et al., 2016). To test whether pulsatile MEKi treatment can improve antigen-specific priming of T cells, we utilized antigen-specific, Pmel-1 transgenic CD8+ T cells pulsed with gp100 peptide. We showed that selumetinib and trametinib reduced antigen-specific activation (CD44+) in a dose-dependent manner in both continuous and pulsatile treatments, which suggests a critical role of pERK in CD8+ T cell priming. However, pulsatile MEKi treatment resulted in more CD44+CD62L− cells than continuous treatment did. This observation is important, because it suggests that pulsatile treatment leads to maintained activation when compared to conventional MEKi treatment. To clearly understand the effects of MEKis in immune priming, future work to dynamically monitor pERK expression and T cell activation marker changes with diverse types of MEKis pulsation is needed. Additionally, *in vivo* studies confirming whether the pulsatile schedule of MEKis enhances priming of T cells need to be pursued further.

Given the observations of T cell phenotypic changes *ex vivo* and *in vivo* in transplantable models, we further evaluated such changes, using a GEMM harboring the human $KRAS^{G12C}$ mutation, one of the most prevalent mutation detected in NSCLC patients. We found that pulsatile treatment with MEKis have a superior anti-tumor effect and delayed drug resistance in comparison with continuous treatment. Consistent with *ex vivo* and *in vivo* transplantable model studies, the tumor-infiltrating T cells showed increased CTLA-4 and a modest upregulation of PD-1 levels, with greater proliferation and activation. In contrast, when we treated $KRAS^{G12C}$ mutant GEMM mice with MEKis continuously, we observed reduced CTLA-4 and PD-1. Considering that the tumor cells were exposed to equal amounts

(F) Survival curve from the selumetinib and anti-CTLA-4 treatment combination in immune-deficient mice (Rag1−/−). The color code is as same as in (F).
(G) Survival of the pulsatile selumetinib and anti-CTLA-4 treatment group.
Survival analysis was done by Log-rank (Mantel-Cox) test. * < 0.05; ** < 0.01. Samples were biological replicates. The experiment was performed 2–3 times, and representative results are shown here.

of MEKis, this confirms that activated T cells resulting from pulsatile MEKi treatment could enhance anti-tumor immunity in KRAS-driven lung cancer.

In all conditions (*ex vivo* and *in vivo* in GEMM and transplantable models), we have observed that pulsatile MEKi treatment increases CTLA-4 and PD-1. Although CTLA-4 is a checkpoint molecule (Hardy and Chaudhri, 1997; Thompson and Allison, 1997; Walunas et al., 1994), counterintuitively, it is also known to be induced during early T cell activation (Chambers et al., 1996). In a similar way, while PD-1 is highly expressed on exhausted T cells, it is also a marker of T cell stimulation (Jin et al., 2011; Kansy et al., 2017; Ngiow et al., 2015). Thus, increased CTLA-4 and PD-1 associated with pulsatile MEKi treatment suggests that CD8+ T cells are more activated, and this is supported by data on Ki67 expression. Moreover, considering that exhausted T cells co-express other co-inhibitory markers like TIM-3 and LAG-3 simultaneously with PD-1, the absence of these co-inhibitory markers on T cells after pulsatile MEKi treatment supports that they are activated rather than exhausted cells. Favorable changes in CTLA-4 after pulsatile MEKi treatment warrant considering how CTLA-4 expression is regulated. It is known that CTLA-4 is regulated by ERK (Tsatsanis et al., 2008), but it is not well understood how CTLA-4 expression is regulated temporally in the presence of MEKis. A future study on the mechanism of CTLA-4 expression regulation under MEKis is necessary.

Improved anti-tumor activity and a more favorable phenotype of CD8+ T cells with increased CTLA-4 expression in the pulsatile group inspired us to test the combination of pulsatile MEKi treatment with an anti-CTLA4 antibody in Kras mutant lung cancer. We show that the combination of pulsatile high doses of selumetinib and CTLA-4 blockade prolonged survival to the greatest extent compared to other monotherapies or combination therapies, supporting that the combination of immune checkpoint blockade with pulsatile MEKis may be a more effective approach to treat Kras lung cancer. This prolonged survival was not present in immune-deficient mice, indicating that it was mediated by the adaptive immune system. A similar pulsatile treatment regimen is also currently under evaluation in a clinic for NSCLC patients with intermittent selumetinib and antibodies targeting CTLA-4 and PD-L1 (ClinicalTrial.gov: NCT03581487). It should be noted that, since the trial did not stratify for co-mutations in addition to KRAS, MEKi alone, which targets downstream of KRAS, may not be enough to restrain tumors with a KRAS mutation together with other co-mutations, even when combined with immunotherapy.

In this study, we have tested MEK inhibition with selumetinib and trametinib. However, other MEKis with variations in potency, target specificity, and $T_{1/2}$ (elimination half-life) are being used (e.g., cobimetinib and binimetinib) or are in development (Caunt et al., 2015). Based on our findings, these should also be tested using different dosing and scheduling regimens to potentially allow for more effective cancer cell growth control and durable immune microenvironment activation.

In this study, we show that the pulsatile schedule alters the tumor microenvironment favorably by activating T cells and providing an advantageous anti-tumor effect in Kras-driven lung cancer models. This schedule provides a therapeutic window for immune checkpoint blockade to improve MEKis for the treatment of KRAS-driven NSCLC patients.

STAR★METHODS

Detailed methods are provided in the online version of this paper and include the following:

- KEY RESOURCES TABLE
- CONTACT FOR REAGENT AND RESOURCE SHARING
- EXPERIMENTAL MODEL AND SUBJECT DETAILS
  - Cell lines and transplantable mouse model
  - GEMM model studies
- METHOD DETAILS
  - *In vitro* MEKis treatment
  - Western blot
  - *Ex vivo* T cell priming with MEKis treatment
  - MRI quantification
  - Tumor-infiltrating immune cells isolation and analysis
  - Transcriptome analysis
  - Flow cytometry analysis
  - Cytokine profiling analysis
  - Immunohistochemistry (IHC) staining and analyses
- QUANTIFICATION AND STATISTICAL ANALYSIS
  - Statistical Analysis
- DATA AND SOFTWARE AVAILABILITY
  - Data Resources

SUPPLEMENTAL INFORMATION

Supplemental Information can be found online at https://doi.org/10.1016/j.celrep.2019.03.066.

ACKNOWLEDGMENTS

We thank Nouraiz Falik for the work on validation animal experiments. This research was funded in part through a Stand Up To Cancer-American Cancer Society Lung Cancer Dream Team Translational Research Grant (SU2C-AACR-DT17-15); NIH-NCI Cancer Center Support grant P30 CA008748; the Ludwig Collaborative and Swim Across America Laboratory; Memorial Sloan Kettering Cancer Center, United States; the Parker Institute for Cancer Immunotherapy, Memorial Sloan Kettering Cancer Center; the Department of Medicine, Memorial Sloan Kettering Cancer Center; and Weill Cornell Medicine, United States.

AUTHOR CONTRIBUTIONS

Conceptualization, H.C., J.D., S.L., P.D.S., K.-K.W., T.M., and J.D.W.; Validation, H.C., J.D., S.L., L.D., and H.Z.; Formal Analysis, H.C., J.D., S.L., S.H., and D.R.; Investigation, H.C., J.D., S.L., T.S., E.J.B., and J.B.; Writing – Original Draft, H.C., J.D., and S.L.; Writing – Review & Editing, H.C., J.D., S.L., T.S., E.A.A., T.M., and J.D.W.; Visualization, H.C., J.D., and S.L.; Supervision, T.M., J.D.W., and K.-K.W.

DECLARATION OF INTERESTS

P.D.S. is an employee and shareholder of AstraZeneca.

T.M. is a cofounder and holds an equity in IMVAQ Therapeutics. He is a consultant of Immunos Therapeutics and Pfizer. He has research support from Bristol-Myers Squibb; Surface Oncology; Kyn Therapeutics; Infinity Pharmaceuticals, Inc.; Peregrine Pharmaceuticals, Inc.; Adaptive Biotechnologies; Leap Therapeutics, Inc.; and Aprea. He has patents on applications related to

work on oncolytic viral therapy, alpha virus-based vaccine, neo antigen modeling, CD40, GITR, OX40, PD-1, and CTLA-4.

K.K.W. is a founder and equity holder of G1 Therapeutics. He has sponsored research agreements with MedImmune, Takeda, TargImmune, and BMS. He also has consulting and sponsored research agreements with AstraZeneca, Janssen, Pfizer, Novartis, Merck, Ono, and Array.

J.D.W. is a consultant for Adaptive Biotech; Advaxis; Amgen; Apricity; Array BioPharma; Ascentage Pharma; Astellas; Bayer; Beigene; Bristol Myers Squibb; Celgene; Chugai; Elucida; Eli Lilly; F Star; Genentech; Imvaq; Janssen; Kleo Pharma; Linneaus; MedImmune; Merck; Neon Therapuetics; Ono; Polaris Pharma; Polynoma; Psioxus; Puretech; Recepta; Trieza; Sellas Life Sciences; Serametrix; Surface Oncology; and Syndax. He has research support from Bristol Myers Squibb, Medimmune, and Genentech. He holds equity in Potenza Therapeutics; Tizona Pharmaceuticals; Adaptive Biotechnologies; Elucida; Imvaq; Beigene; Trieza; and Linneaus and has an honorarium from Esanex. He has patents of xenogeneic DNA vaccines (royalties); alphavirus replicon particles expressing TRP2; myeloid-derived suppressor cell (MDSC) assay (royalties); Newcastle disease viruses for cancer therapy; a genomic signature to identify responders to ipilimumab in melanoma; engineered vaccinia viruses for cancer immunotherapy; an anti-CD40 agonist monoclonal antibody (mAb) fused to monophosphoryl lipid A (MPL) for cancer therapy; CAR T cells targeting differentiation antigens as means to treat cancer; an anti-PD1 antibody; anti-CTLA4 antibodies; and anti-GITR antibodies and methods of use thereof.

The other authors declare no competing interests.

Received: July 26, 2018
Revised: February 1, 2019
Accepted: March 18, 2019
Published: April 16, 2019

REFERENCES

Andrzejewski, S., Klimcakova, E., Johnson, R.M., Tabariès, S., Annis, M.G., McGuirk, S., Northey, J.J., Chénard, V., Sriram, U., Papadopoli, D.J., et al. (2017). PGC-1α promotes breast cancer metastasis and confers bioenergetic flexibility against metabolic drugs. Cell Metab. *26*, 778–787.e5.

Bolstad, B.M., Irizarry, R.A., Astrand, M., and Speed, T.P. (2003). A comparison of normalization methods for high density oligonucleotide array data based on variance and bias. Bioinformatics *19*, 185–193.

Borghaei, H., Paz-Ares, L., Horn, L., Spigel, D.R., Steins, M., Ready, N.E., Chow, L.Q., Vokes, E.E., Felip, E., Holgado, E., et al. (2015). Nivolumab versus docetaxel in advanced nonsquamous non-small-cell lung cancer. N. Engl. J. Med. *373*, 1627–1639.

Brahmer, J., Reckamp, K.L., Baas, P., Crinò, L., Eberhardt, W.E.E., Poddubskaya, E., Antonia, S., Pluzanski, A., Vokes, E.E., Holgado, E., et al. (2015). Nivolumab versus docetaxel in advanced squamous-cell non-small-cell lung cancer. N. Engl. J. Med. *373*, 123–135.

Brant, R., Sharpe, A., Liptrot, T., Dry, J.R., Harrington, E.A., Barrett, J.C., Whalley, N., Womack, C., Smith, P., and Hodgson, D.R. (2017). Clinically viable gene expression assays with potential for predicting benefit from MEK inhibitors. Clin. Cancer Res. *23*, 1471–1480.

Brea, E.J., Oh, C.Y., Manchado, E., Budhu, S., Gejman, R.S., Mo, G., Mondello, P., Han, J.E., Jarvis, C.A., Ulmert, D., et al. (2016). Kinase regulation of human MHC class I molecule expression on cancer cells. Cancer Immunol. Res. *4*, 936–947.

Callahan, M.K., Masters, G., Pratilas, C.A., Ariyan, C., Katz, J., Kitano, S., Russell, V., Gordon, R.A., Vyas, S., Yuan, J., et al. (2014). Paradoxical activation of T cells via augmented ERK signaling mediated by a RAF inhibitor. Cancer Immunol. Res. *2*, 70–79.

Carvalho, B.S., and Irizarry, R.A. (2010). A framework for oligonucleotide microarray preprocessing. Bioinformatics *26*, 2363–2367.

Caunt, C.J., Sale, M.J., Smith, P.D., and Cook, S.J. (2015). MEK1 and MEK2 inhibitors and cancer therapy: the long and winding road. Nat. Rev. Cancer *15*, 577–592.

Chambers, C.A., Krummel, M.F., Boitel, B., Hurwitz, A., Sullivan, T.J., Fournier, S., Cassell, D., Brunner, M., and Allison, J.P. (1996). The role of CTLA-4 in the regulation and initiation of T-cell responses. Immunol. Rev. *153*, 27–46.

Chen, Z., Cheng, K., Walton, Z., Wang, Y., Ebi, H., Shimamura, T., Liu, Y., Tupper, T., Ouyang, J., Li, J., et al. (2012). A murine lung cancer co-clinical trial identifies genetic modifiers of therapeutic response. Nature *483*, 613–617.

Choi, H., Sheng, J., Gao, D., Li, F., Durrans, A., Ryu, S., Lee, S.B., Narula, N., Rafii, S., Elemento, O., et al. (2015). Transcriptome analysis of individual stromal cell populations identifies stroma-tumor crosstalk in mouse lung cancer model. Cell Rep. *10*, 1187–1201.

D'Souza, W.N., Chang, C.-F., Fischer, A.M., Li, M., and Hedrick, S.M. (2008). The Erk2 MAPK regulates CD8 T cell proliferation and survival. J. Immunol. *181*, 7617–7629.

Das Thakur, M., Salangsang, F., Landman, A.S., Sellers, W.R., Pryer, N.K., Levesque, M.P., Dummer, R., McMahon, M., and Stuart, D.D. (2013). Modelling vemurafenib resistance in melanoma reveals a strategy to forestall drug resistance. Nature *494*, 251–255.

Dushyanthen, S., Teo, Z.L., Caramia, F., Savas, P., Mintoff, C.P., Virassamy, B., Henderson, M.A., Luen, S.J., Mansour, M., Kershaw, M.H., et al. (2017). Agonist immunotherapy restores T cell function following MEK inhibition improving efficacy in breast cancer. Nat. Commun. *8*, 606.

Ebert, P.J.R., Cheung, J., Yang, Y., McNamara, E., Hong, R., Moskalenko, M., Gould, S.E., Maecker, H., Irving, B.A., Kim, J.M., et al. (2016). MAP kinase inhibition promotes T cell and anti-tumor activity in combination with PD-L1 checkpoint blockade. Immunity *44*, 609–621.

Fernández-Medarde, A., and Santos, E. (2011). Ras in cancer and developmental diseases. Genes Cancer *2*, 344–358.

Friday, B.B., and Adjei, A.A. (2008). Advances in targeting the Ras/Raf/MEK/Erk mitogen-activated protein kinase cascade with MEK inhibitors for cancer therapy. Clin. Cancer Res. *14*, 342–346.

Garon, E.B., Rizvi, N.A., Hui, R., Leighl, N., Balmanoukian, A.S., Eder, J.P., Patnaik, A., Aggarwal, C., Gubens, M., Horn, L., et al.; KEYNOTE-001 Investigators (2015). Pembrolizumab for the treatment of non-small-cell lung cancer. N. Engl. J. Med. *372*, 2018–2028.

Greystoke, A., Steele, N., Arkenau, H.T., Blackhall, F., Md Haris, N., Lindsay, C.R., Califano, R., Voskoboynik, M., Summers, Y., So, K., et al. (2017). SELECT-3: a phase I study of selumetinib in combination with platinum-doublet chemotherapy for advanced NSCLC in the first-line setting. Br. J. Cancer *117*, 938–946.

Hardy, K., and Chaudhri, G. (1997). Activation and signal transduction via mitogen-activated protein (MAP) kinases in T lymphocytes. Immunol. Cell Biol. *75*, 528–545.

Hellmann, M.D., Rizvi, N.A., Goldman, J.W., Gettinger, S.N., Borghaei, H., Brahmer, J.R., Ready, N.E., Gerber, D.E., Chow, L.Q., Juergens, R.A., et al. (2017). Nivolumab plus ipilimumab as first-line treatment for advanced non-small-cell lung cancer (CheckMate 012): results of an open-label, phase 1, multicohort study. Lancet Oncol. *18*, 31–41.

Holmström, T.H., Schmitz, I., Söderström, T.S., Poukkula, M., Johnson, V.L., Chow, S.C., Krammer, P.H., and Eriksson, J.E. (2000). MAPK/ERK signaling in activated T cells inhibits CD95/Fas-mediated apoptosis downstream of DISC assembly. EMBO J. *19*, 5418–5428.

Irizarry, R.A., Bolstad, B.M., Collin, F., Cope, L.M., Hobbs, B., and Speed, T.P. (2003a). Summaries of Affymetrix GeneChip probe level data. Nucleic Acids Res. *31*, e15.

Irizarry, R.A., Hobbs, B., Collin, F., Beazer-Barclay, Y.D., Antonellis, K.J., Scherf, U., and Speed, T.P. (2003b). Exploration, normalization, and summaries of high density oligonucleotide array probe level data. Biostatistics *4*, 249–264.

Jamal-Hanjani, M., Wilson, G.A., McGranahan, N., Birkbak, N.J., Watkins, T.B.K., Veeriah, S., Shafi, S., Johnson, D.H., Mitter, R., Rosenthal, R., et al.; TRACERx Consortium (2017). Tracking the evolution of non-small-cell lung cancer. N. Engl. J. Med. *376*, 2109–2121.

Jin, H.T., Ahmed, R., and Okazaki, T. (2011). Role of PD-1 in regulating T-cell immunity. Curr. Top. Microbiol. Immunol. *350*, 17–37.

Jones-Bolin, S.E., Johansson, E., Palmisano, W.A., Anderson, M.W., Wiest, J.S., and Belinsky, S.A. (1998). Effect of promoter and intron 2 polymorphisms on murine lung K-ras gene expression. Carcinogenesis *19*, 1503–1508.

Kane, L.P., Lin, J., and Weiss, A. (2000). Signal transduction by the TCR for antigen. Curr. Opin. Immunol. *12*, 242–249.

Kansy, B.A., Concha-Benavente, F., Srivastava, R.M., Jie, H.-B., Shayan, G., Lei, Y., Moskovitz, J., Moy, J., Li, J., Brandau, S., et al. (2017). PD-1 status in CD8+ T cells associates with survival and anti-PD-1 therapeutic outcomes in head and neck cancer. Cancer Res. *77*, 6353–6364.

Lastwika, K.J., Wilson, W., 3rd, Li, Q.K., Norris, J., Xu, H., Ghazarian, S.R., Kitagawa, H., Kawabata, S., Taube, J.M., Yao, S., et al. (2016). Control of PD-L1 expression by oncogenic activation of the AKT-mTOR pathway in non-small cell lung cancer. Cancer Res. *76*, 227–238.

Li, S., Liu, S., Deng, J., Akbay, E.A., Hai, J., Ambrogio, C., Zhang, L., Zhou, F., Jenkins, R.W., Adeegbe, D.O., et al. (2018). Assessing therapeutic efficacy of MEK inhibition in a KRAS^{G12C}-driven mouse model of lung cancer. Clin. cancer res. *24*, 4854–4864.

Liu, L., Mayes, P.A., Eastman, S., Shi, H., Yadavilli, S., Zhang, T., Yang, J., Seestaller-Wehr, L., Zhang, S.Y., Hopson, C., et al. (2015a). The BRAF and MEK inhibitors dabrafenib and trametinib: effects on immune function and in combination with immunomodulatory antibodies targeting PD-1, PD-L1, and CTLA-4. Clin. Cancer Res. *21*, 1639–1651.

Liu, X., Yu, X., Xie, J., Zhan, M., Yu, Z., Xie, L., Zeng, H., Zhang, F., Chen, G., Yi, X., and Zheng, J. (2015b). ANGPTL2/LILRB2 signaling promotes the propagation of lung cancer cells. Oncotarget *6*, 21004–21015.

Lovly, C.M., and Carbone, D.P. (2011). Lung cancer in 2010: one size does not fit all. Nat. Rev. Clin. Oncol. *8*, 68–70.

Manchado, E., Weissmueller, S., Morris, J.P., 4th, Chen, C.C., Wullenkord, R., Lujambio, A., de Stanchina, E., Poirier, J.T., Gainor, J.F., Corcoran, R.B., et al. (2016). A combinatorial strategy for treating KRAS-mutant lung cancer. Nature *534*, 647–651.

Nassal, D.M., Wan, X., Liu, H., Maleski, D., Ramirez-Navarro, A., Moravec, C.S., Ficker, E., Laurita, K.R., and Deschênes, I. (2017). KChIP2 is a core transcriptional regulator of cardiac excitability. eLife *6*, e17304.

Ngiow, S.F., Young, A., Jacquelot, N., Yamazaki, T., Enot, D., Zitvogel, L., and Smyth, M.J. (2015). A threshold level of intratumor CD8+ T-cell PD1 expression dictates therapeutic response to anti-PD1. Cancer Res. *75*, 3800–3811.

Ostrem, J.M., Peters, U., Sos, M.L., Wells, J.A., and Shokat, K.M. (2013). K-Ras(G12C) inhibitors allosterically control GTP affinity and effector interactions. Nature *503*, 548–551.

Overwijk, W.W., Theoret, M.R., Finkelstein, S.E., Surman, D.R., de Jong, L.A., Vyth-Dreese, F.A., Dellemijn, T.A., Antony, P.A., Spiess, P.J., Palmer, D.C., et al. (2003). Tumor regression and autoimmunity after reversal of a functionally tolerant state of self-reactive CD8+ T cells. J. Exp. Med. *198*, 569–580.

Planchard, D., Smit, E.F., Groen, H.J.M., Mazieres, J., Besse, B., Helland, Å., Giannone, V., D'Amelio, A.M., Jr., Zhang, P., Mookerjee, B., and Johnson, B.E. (2017). Dabrafenib plus trametinib in patients with previously untreated $BRAF^{V600E}$-mutant metastatic non-small-cell lung cancer: an open-label, phase 2 trial. Lancet Oncol. *18*, 1307–1316.

Poon, E., Mullins, S., Watkins, A., Williams, G.S., Koopmann, J.O., Di Genova, G., Cumberbatch, M., Veldman-Jones, M., Grosskurth, S.E., Sah, V., et al. (2017). The MEK inhibitor selumetinib complements CTLA-4 blockade by reprogramming the tumor immune microenvironment. J. Immunother. Cancer *5*, 63.

Reck, M., Rodríguez-Abreu, D., Robinson, A.G., Hui, R., Csőszi, T., Fülöp, A., Gottfried, M., Peled, N., Tafreshi, A., Cuffe, S., et al.; KEYNOTE-024 Investigators (2016). Pembrolizumab versus chemotherapy for PD-L1-positive non-small-cell lung cancer. N. Engl. J. Med. *375*, 1823–1833.

Riely, G.J., Marks, J., and Pao, W. (2009). KRAS mutations in non-small cell lung cancer. Proc. Am. Thorac. Soc. *6*, 201–205.

Rincón, M., Flavell, R.A., and Davis, R.J. (2001). Signal transduction by MAP kinases in T lymphocytes. Oncogene *20*, 2490–2497.

Samatar, A.A., and Poulikakos, P.I. (2014). Targeting RAS-ERK signalling in cancer: promises and challenges. Nat. Rev. Drug Discov. *13*, 928–942.

Shah, N.P., Kasap, C., Weier, C., Balbas, M., Nicoll, J.M., Bleickardt, E., Nicaise, C., and Sawyers, C.L. (2008). Transient potent BCR-ABL inhibition is sufficient to commit chronic myeloid leukemia cells irreversibly to apoptosis. Cancer Cell *14*, 485–493.

Solit, D.B., She, Y., Lobo, J., Kris, M.G., Scher, H.I., Rosen, N., and Sirotnak, F.M. (2005). Pulsatile administration of the epidermal growth factor receptor inhibitor gefitinib is significantly more effective than continuous dosing for sensitizing tumors to paclitaxel. Clin. Cancer Res. *11*, 1983–1989.

Soria, J.C., Fülop, A., Maciel, C., Fischer, J.R., Girotto, G., Lago, S., Smit, E., Ostoros, G., Eberhardt, W.E.E., Lishkovska, P., et al. (2017). SELECT-2: a phase II, double-blind, randomised, placebo-controlled study to assess the efficacy of selumetinib plus docetaxel as a second-line treatment for patients with advanced or metastatic non-small cell lung cancer. Ann. Oncol. *28*, 3028–3036.

Stinchcombe, T.E., and Johnson, G.L. (2014). MEK inhibition in non-small cell lung cancer. Lung Cancer *86*, 121–125.

Sun, C., Hobor, S., Bertotti, A., Zecchin, D., Huang, S., Galimi, F., Cottino, F., Prahallad, A., Grernrum, W., Tzani, A., et al. (2014). Intrinsic resistance to MEK inhibition in KRAS mutant lung and colon cancer through transcriptional induction of ERBB3. Cell Rep. *7*, 86–93.

Swanton, C., and Govindan, R. (2016). Clinical implications of genomic discoveries in lung cancer. N. Engl. J. Med. *374*, 1864–1873.

Thompson, C.B., and Allison, J.P. (1997). The emerging role of CTLA-4 as an immune attenuator. Immunity *7*, 445–450.

Tsatsanis, C., Vaporidi, K., Zacharioudaki, V., Androulidaki, A., Sykulev, Y., Margioris, A.N., and Tsichlis, P.N. (2008). Tpl2 and ERK transduce antiproliferative T cell receptor signals and inhibit transformation of chronically stimulated T cells. Proc. Natl. Acad. Sci. USA *105*, 2987–2992.

Walunas, T.L., Lenschow, D.J., Bakker, C.Y., Linsley, P.S., Freeman, G.J., Green, J.M., Thompson, C.B., and Bluestone, J.A. (1994). CTLA-4 can function as a negative regulator of T cell activation. Immunity *1*, 405–413.

Weiss, A., and Littman, D.R. (1994). Signal transduction by lymphocyte antigen receptors. Cell *76*, 263–274.

Wolchok, J.D., Kluger, H., Callahan, M.K., Postow, M.A., Rizvi, N.A., Lesokhin, A.M., Segal, N.H., Ariyan, C.E., Gordon, R.A., Reed, K., et al. (2013). Nivolumab plus ipilimumab in advanced melanoma. N. Engl. J. Med. *369*, 122–133.

Zeng, M., Lu, J., Li, L., Feru, F., Quan, C., Gero, T.W., Ficarro, S.B., Xiong, Y., Ambrogio, C., Paranal, R.M., et al. (2017). Potent and selective covalent quinazoline inhibitors of KRAS G12C. Cell Chem. Biol. *24*, 1005–1016.e3.

STAR★METHODS

KEY RESOURCES TABLE

REAGENT or RESOURCE	SOURCE	IDENTIFIER
Antibodies		
phospho-p44/42 MAPK (Erk1/2) (20G11)	Cell Signaling Technology	Cat# 4376; RRID:AB_331772
phospho-p44/42 MAPK (Erk1/2) (E10)	Cell Signaling Technology	Cat# 9106; RRID:AB_331768
phospho-p44/42 MAPK (Erk1/2) (D13.14.4E)	Cell Signaling Technology	Cat# 4370; RRID:AB_2315112
P44-42 MAPK (Erk1/2)	Cell Signaling Technology	Cat#9102; RRID:AB_330744
CD11b (M1/70)	BioLegend	Cat# 101224; RRID:AB_755986
CD11b (M1/70.15)	Invitrogen	Cat# RM2817; RRID:AB_1464525
CD11c (N418)	BioLegend	Cat# 117324; RRID:AB_830649
PD-1 (J43)	eBioscience	Cat# 11-9985-85: RRID:AB_465473
PD-1 (29F.1A12)	Biolegend	Cat# 135215; RRID:AB_10696422
CTLA-4 (UC10-4B9)	ThermoFisher	Cat# 12-1522-81; RRID:AB_465878
CTLA-4 (UC10-4B9)	eBioscience	Cat# 17-1522-82; RRID:AB_2016700
LAG-3 (C9B7W)	BioLegend	Cat# 125209; RRID:AB_10639935
LAG-3 (eBioC9B7W)	eBioscience	Cat# 48-2231-82; RRID:AB_11149866
PD-L1 (10F.9G2)	BioLegend	Cat# 124311; RRID:AB_10612935
Armenian Hamster IgG (eBio299Arm)	ThermoFisher	Cat# 12-4888-81; RRID:AB_470073
CD3 (17A2, for flow cytometry)	BioLegend	Cat# 100214; RRID:AB_493645
CD3 (17A2, for flowcytometry)	BioLegends	Cat# 100221; RRID:AB_2057374
CD3 (145-2C11)	BD PharMingen	Cat# 561108/551163; RRID:AB_10562558/ RRID:AB_394082
EpCAM (G8.8)	BioLegend	Cat# 118215; RRID:AB_1236477
CD4 (GK1.5)	BioLegend	Cat# 100411; RRID:AB_312696
CD4 (GK1.5)	BioLegend	Cat# 100406; RRID:AB_312691
CD45 (30-F11)	BioLegend	Cat# 103108; RRID:AB_312973
CD8 (53-6.7)	BioLegends	Cat# 100734; RRID:AB_2075238
CD8 (5H19)	Invitrogen	Cat # MCD0817; RRID:AB_10374589
FoxP3 (FJK-16 s)	eBioscience	Cat# 17-5773-80; RRID:AB_469456
FoxP3 (FJK-16 s)	eBioscience	Cat# 25-5773-82; RROD:AB_891552
IFN-γ (XMG1.2)	BioLegend	Cat# 505825; RRID:AB_1595591
Ki-67 (16A8)	BioLegend	Cat# 652411; RRID:AB_2562663
Ki-67 (SolA15)	Invitrogen	Cat# 48-5698-82; RRID:AB_11149124
IgG1 (RTK2071)	BioLegend	Cat# 400415; RRID:AB_326521
IgG1 (RTK2071)	BioLegend	Cat# 400411; RRID:AB_326517
IgG2a (eBR2a)	eBioscience	Cat# 12-4321-81; RRID:AB_470051
IgG2a (eBR2a)	eBioscience	Cat# 17-4321-81; RRID:AB_470181
IgG2a (RTK2758)	BioLegend	Cat# 400521; RRID:AB_326542
IgG2a (RTK2758)	BioLegend	Cat# 400535; RRID:AB_10933427
TIM3 (RMT3-23)	eBioscience	Cat# 12-5870-81; RRID:AB_465973
Tbet (eBio4B10)	eBioscience	Cat# 12-5825-82; RRID:AB_925761
ICOS (c398.4A)	eBioscience	Cat# 11-9949-82; RRID:AB_465458
4-1BB (17B5)	eBioscience	Cat# 12-1371-83; RRID:AB_465865
GITR (DTA-1)	eBioscience	Cat# 48-5874-82; RRID:AB_1944394
OX40 (OX-86)	eBioscience	Cat# 17-1341-82; RRID:AB_10717260

(*Continued on next page*)

Continued

REAGENT or RESOURCE	SOURCE	IDENTIFIER
CD62L (MEL-14)	eBioscience	Cat# 56-0621-82; RRID:AB_494003
CD44 (IM7)	BD PharMingen	Cat# 559250; RRID:AB_398661
Anti Fcgamma, purified	MSK Antibody and Bioresource Core	Clone: 2.4G2
CD3 (for *in vitro* T cell activation)	MSK Antibody and Bioresource Core	Clone: 145-2C11
CD28 (for *in vitro* T cell activation)	MSK Antibody and Bioresource Core	Clone: 37N
mouse anti-CTLA-4 (9H10, *in vivo* antibody)	Bioxcell	Cat# BE0131; RRID:AB_10950184
mouse anti-CTLA-4 (9D9, *in vivo* antibody)	Bioxcell	Cat# BE0164; RRID:AB_10949609
Syrian Hamster IgG	Bioxcell	Cat# BE0087; RRID:AB_1107782
InVivoMAb mouse IgG2b isotype control (MCP-11)	Bioxcell	Cat# BE0086; RRID:AB_1107791
mouse anti-PD-1 (RMP1-14, for *in vivo* experiment)	Bioxcell	Cat# BE0146: RRID:AB_10949053
InVivoMAb rat IgG2a isotype control (2A3)	Bioxcell	Cat# BE0089; RRID:AB_1107769
NK1.1 (PK136, *in vivo* antibody)	Bioxcell	Cat#BE0036; RRID: AB_1107737
Bacterial and Virus Strains		
Ad5CMVCre	UI Viral Vector Core Web	VVC-U of Iowa-5
Chemicals, Peptides, and Recombinant Proteins		
Selumetinib	Selleckchem	Cat# S1008
Trametinib	Selleckchem	Cat# S2673
gp100 peptide, human	Anaspec Inc	Cat# AS-62589
Recombinant mouse IL-2	eBioscience	Cat# 14-8021-64
Fixable viability dye (for flow cytometry)	eBioscience	Cat# 65-0866-14
Critical Commercial Assays		
LIVE/DEAD Fixable Aqua Dead Cell Stain Kit	ThermoFisher	Cat# L34966
CD5 (Ly-1) MicroBeads, mouse	Miltenyi	Cat# 130-049-301
Luminex cytokine analysis (mouse)-MILLIPLEX MAP Mouse Cytokine/Chemokine Magnetic Bead Panel - Immunology Multiplex Assay	Millipore	Cat# MCYTMAG-70K-PX32
Mouse Cytokine 23-plex Assay	Bio-Rad	#m60009rdpd
Cell titer Glo luminescent cell viability assay	Promega	G7571
QUICK RNA FFPE Kit	Zymo Research	R1008
Deposited Data		
Affymetrix transcriptome data	NCBI Gene Expression Omnibus	GEO: GSE126202
Experimental Models: Cell Lines		
Mouse; CL13	Dr. Phillip A. Dennis	PMID: 26637667
Mouse; CL25	Dr. Phillip A. Dennis	PMID: 26637667
Mouse; IO33	Dr. Phillip A. Dennis	PMID: 26637667
Mouse; HKP1	Dr. Vivek Mittal laboratory (WCMC)	PMID: 25704820
Mouse; LLC	ATCC	ATCC® CRL-1642
Mouse; $Kras^{G12D}Trp53^{fl/fl}$ cell line from GEMM	Dr. Kwok-Kin Wong laboratory (NYU)	N/A
Mouse: primary T lymphocytes	This study	N/A
Experimental Models: Organisms/Strains		
Mouse; $KRAS^{LSL-G12C}$ GEMM	Dr. Kwok-Kin Wong laboratory (NYU)	PMID: 29945997
Mouse; Pmel TCR transgenic mouse	Dr. Nicholas Restifo laboratory (NIH)	PMID: 12925674
Mouse; Rag1−/−; B6.129S7-Rag1tm1Mom/J	Jax lab	Jax 002216
Mouse; C57BL/6J; C57BL/6J	Jax lab	Jax 000664
Software and Algorithms		
3D slicer	Online download	https://www.slicer.org/
GraphGad Prism 7	Online download	https://www.graphpad.com/scientific-software/prism/

(*Continued on next page*)

Continued

REAGENT or RESOURCE	SOURCE	IDENTIFIER
FlowJo v.10	Online download	https://www.flowjo.com/solutions/flowjo/downloads
IVIS Living image software v. 4.4	Perkin Elmer	http://www.perkinelmer.com/category/in-vivo-imaging-software?gclid=EAIaIQobChMIoK2N_LKW4AIVk4TICh0LeAU9EAAYASACEgLwr_D_BwE
Transcriptome Analysis Console (TAC) Software v.4.0	ThermoFisher Scientific	https://www.thermofisher.com/us/en/home/life-science/microarray-analysis/microarray-analysis-instruments-software-services/microarray-analysis-software/affymetrix-transcriptome-analysis-console-software.html
Robust Multi-array Average (RMA) procedure	Irizarry et al., 2003a	https://www.rdocumentation.org/packages/affy/versions/1.50.0/topics/rma
Other		
MRI imaging	Dana-Farber Cancer Institute's Lurie Family Imaging Center	http://www.lfic.dfci.harvard.edu/about
Affymetrix microarray Assay	ThermoFisher Scientific	Mouse Clariom D Pico assay

CONTACT FOR REAGENT AND RESOURCE SHARING

Further information and requests for resources and reagents should be directed to and will be fulfilled by the Lead Contact, Taha Merghoub (merghout@mskcc.org).

EXPERIMENTAL MODEL AND SUBJECT DETAILS

Cell lines and transplantable mouse model

CL13, CL25, IO33 cells lines (Jones-Bolin et al., 1998) were obtained from Dr. Phillip A. Dennis (Lastwika et al., 2016). They were cultured in RPMI with 7.5% FBS and Pen/Strep. The HKP1 cell line was obtained from Dr. Vivek Mittal at Weill Cornell Medical College (Choi et al., 2015). LLC (Lewis Lung Carcinoma) was obtained from ATCC (CRL-1642). HKP1 and LLC were cultured in DMEM with 10% fetal calf serum, L-Glutamine, sodium pyruvate, and Pen/Strep. Sex of CL13, CL25, IO33, HKP1, and LLC is female based on our sequencing analysis. $Kras^{G12D}p53^{f/f}$ cell line was derived from male mouse in Dr. Kwok-Kin Wong's laboratory and cultured in RPMI with 7.5% FBS and Pen/Strep. The cell lines have been kept in culture for a limited number of passage. Cell lines are also routinely mycoplasma tested and each new cell line is mycoplasma tested by the monoclonal core facility at MSK. Cell lines are also tested for Mouse antibody production (MAP) routinely at MSK.

All animal studies were reviewed and approved by the Institutional Animal Care and Use Committee (IACUC) at the Memorial Sloan Kettering Cancer Center and Dana-Farber Cancer Institute. All mice for transplantable model were 6 −12 week old of age and females and tumor-bearing mice were randomized before selumetinib treatment (5 mice per group for flow cytometry analysis, 10 mice per group for survival analysis).Transplantable lung cancer was generated by intravenous injection of 1×10^5 HKP1 cells into C57BL/6J (Jax 00664) mice and monitored using the IVIS Spectrum *in vivo* imaging system (Perkin Elmer). 50ul of 30 mg/ml D-luciferine (Perkin Elmer) was injected retro-orbitally under anesthesia using isoflurane and mice were then placed supine in an imaging chamber for imaging. Another transplantable model was generated by subcutaneous injection of 500,000 - 1,000,000 LLC cells in the flank of C57BL/6J (Jax 00664) mice or Rag1−/− (Jax 002216) and tumor growth was measured by calipers. Mice were treated with selumetinib (Selleckchem, Houston, TX USA) from day 5 or day 7 to examine effect of MEKis on tumor growth and survival. Selumetinib was prepared in corn oil and administered by oral gavage twice a day as 25mg/kg for the continuous group daily and 25mg/kg or 300mg/kg for the cyclical pulsatile group according to a planned pulsatile schedule. Survival was analyzed based on the approved humane endpoints (distress and tumor size limit). 100 ug of anti-CTLA-4 was administered to a mouse twice a week for 2–3 weeks intraperitoneally with 9H10 clone for first three doses, then 9D9 clone for rest of doses. 250 ug of anti-PD-1 (RMP1-14) was administered to a mouse twice a week for three weeks intraperitoneally. To deplete NK cells, 200 ug of anti-NK1.1 antibody (PK-136) was injected twice a week for three weeks intraperitoneally.

GEMM model studies

All animal studies were reviewed and approved by the Institutional Animal Care and Use Committee (IACUC) at the Dana-Farber Cancer Institute and New York University School of Medicine (NYUSoM). The genetically engineered mouse model (GEMM) harbors a

conditional activating mutation of the human version of KRAS (*KRAS*$^{LSL\text{-}G12C/+}$) at the collagen I locus (Li et al., 2018) . CRE recombinase was induced through intranasal inhalation of 2.5x10^6 p.f.u. adeno-Cre (University of Iowa adenoviral core). Lung adenocarcinoma appeared 6 weeks after induction. For drug treatment studies in GEMM models, age matched littermates (15 – 21-week-old) were induced at the same time and tumor burden was monitored by MRI. Once the tumor size reached 500 mm^3 (at about 12 weeks after adenoviral inoculation), mice were randomly assigned to experimental groups. We did not observe gender bias response between male and female mice, in terms of tumor growth and response to drug treatment. Mice were evaluated by MRI imaging to quantify lung tumor burden before and after drug treatment. Mice were treated with either vehicle, or 25 mg/kg selumetinib twice daily by oral gavage using either continuous (every day for 3 weeks) or cyclical pulsatile (one week on, one week off) dosing schedule. PFS was analyzed based on the standard criteria in clinical trials. Briefly, PFS was the duration between treatment start and progression, which was defined by increase of tumor size compared to the previous scan of radiological CT and the appearance of new lesions.

METHOD DETAILS

In vitro MEKis treatment

Selumetinib or trametnib (Sellekchem) were added to tumor cells in 96-well plates. Viability was measured using the CellTiter Glo luminescent viability kit (Promega) after 72 hr using a Wallace plate reader (Molecular Probe). To determine pERK after MEKis treatment, Kras mutant lung tumor cell lines and splenocytes collected from HKP1 tumor bearing mice were treated with selumetinib or trametinib for 2 hr at 37C. Selumetinib and trametinib stock solutions were prepared in DMSO and diluted in media. Cells were stimulated with 0.1 ug/ml PMA for 2 min at 37C, then immediately fixed with 4% paraformaldehyde and permeabilized using ice cold 95% methanol. pERK was stained using anti-pERK (#9106, Cell signaling) and goat anti-mouse Ig(H+L)–FITC (SouthernBiotech) by flow cytometry. Washout experiments were done using CD5+ splenocytes from HKP1 tumor bearing mice. CD5+ cells were collected using CD5 microbeads (Miltenyi MACS cell separation system), then seeded in the presence of selumetinib or trametinib into flat bottom 96-well plates pre-coated with anti-CD3 (145-2C11, 1ug/ml) and anti-CD28 (37N, 1ug/ml). After 24hrs, media (RIPA + 7.5% FBS + 0.1% β-mercaptoethanol) was replaced with MEKis (continuous group) or DMSO diluent (wash out group) and the media was changed every day with freshly prepared MEKis. At 72hrs and 96 hr, cells were collected and analyzed by flow cytometry.

Western blot

Trametinib was used *in vitro* at indicated doses in 1% DMSO. Cells were treated for 24 hours before isolating protein. Protein lysate was isolated from cultured cells using RIPA buffer with protease inhibitor (50mM Tris pH 8, 150 mM NaCl, 0.5% sodium deoxycholate, 1% NP-40). Protein quantification was performed using DC Lowry assay. Antibodies for pERK (#4370), ERK1/2 (#9102) were obtained from Cell Signaling Technologies.

Ex vivo T cell priming with MEKis treatment

Pmel-1 TCR transgenic mice (Overwijk et al., 2003) were obtained from Dr. N. Restifo (National Institutes of Health). Splenocytes from a Pmel-1 mouse were stained with 5uM of CFSE (Invitrogen), then seeded at approximately 400,000 cells per well in a U-shape bottom 96 well plate with 1ug/ml of heteroclitic human gp100 peptide (AnaSpec Inc) at day 0 in 0.1% β-mercaptoenthanol supplemented RPMI media with 7.5% FBS. At the same time, splenocytes from another Pmel-1 mouse were set for priming in T175 flask. At day 2 or 3, 20U of mouse IL-2 (eBioscience) was added to the supernatant of the T175 flask that was subsequently used to prepare following treatment groups for the plate. Supernatant with MEKis (selumetinib, trametinib) were added to continuous groups according to the experimental plan. Washout groups were treated with supernatant containing IL-2 and DMSO. At day 4 or 5, 20U/ml of mouse IL-2 supplemented fresh T cell media with or without MEKis was added to support extensive cell growth, and cells were stained and analyzed at day 5 by flow cytometry

MRI quantification

Animals were anesthetized with isoflurane to perform magnetic resonance imaging (MRI) of the lung field using the BioSpec USR70/30 horizontal bore system (Bruker) to scan 24 consecutive sections. Overall tumor volumes within the whole lung were quantified using 3D slicer software to reconstruct MRI volumetric measurements as previously described (Chen et al., 2012). Acquisition of the MRI signal was adapted according to cardiac and respiratory cycles to minimize motion effects during imaging.

Tumor-infiltrating immune cells isolation and analysis

Mice were sacrificed, and lungs were perfused using sterile PBS through heart perfusion from the right ventricle. The whole lung was minced into small pieces and digested in collagenase D (Sigma or GIBCO) and DNase I (Sigma) in Hank's Balanced Salt Solution (HBSS) at 37°C for 30 min. After incubation, the digested tissue was filtered through a 40 um or 70 μm cell strainer (Fisher) to obtain single-cell suspensions. Separated cells were treated with 1X RBC lysis buffer (Biolegend) to lyse red blood cells. Live cells were determined by LIVE/DEAD® fixable aqua dead cell stain kit (Molecular Probes) or Fixable viability dye e506 (eBioscience). The cell pellets were re-suspended in PBS with 2% FBS for flow cytometry analysis. Cells were stained with cell surface markers

as indicated followed by fixation/permeabilization using foxp3 fixation/permeabilization kit (eBioscience). Lung infiltrating immune cells were stained with different combinations of fluorochrome-coupled antibodies and analyzed by FACS analysis.

Transcriptome analysis

RNA was extracted from 6 - 10 FFPE tissue sections using QUICK RNA FFPE kit (Zymo Research). Expression profiling was performed using Affymetrix Clariom D Pico Assay, mouse and analyzed using Transcriptome Analysis Console as previously described. (Andrzejewski et al., 2017; Nassal et al., 2017). Heatmaps were plotted in R using the Robust Multi-array Average (RMA) procedure (Bolstad et al., 2003; Carvalho and Irizarry, 2010; Irizarry et al., 2003a; Irizarry et al., 2003b). Expression values were normalized using Affymetrix mta10 annotation data and gene names were translated to MGI symbols. Heatmaps of signature gene sets were extracted from a study of Brant et al. (Brant et al., 2017).

Flow cytometry analysis

Immune cells obtained via *ex vivo* treatment or *in vivo* were collected and processed as single-cell suspensions and stained with antibodies against mouse CD3 (145-2C11), CD62L (MEL-14), CD44 (IM7), T-bet (eBio4B10), CD45 (30-F11), PD-1 (J43), 4-1BB (17B5), CTLA4 (UC10-4B9), Ki67 (SolA15), Foxp3 (FJK-16 s), CD4 (GK1.5), CD8 (3B5), and fixable viability dye 506 (eBioscience) for *ex vivo* studies; and antibodies against mouse CD3 (17A2), CD4 (GK1.5), CD8 (53-6.7, 5H19), Foxp3 (FJK-16 s), CD11b (M1/70), CD11c (N418), Epcam (G8.8), CD279 (PD-1, 29F.1A12, J43), CD152 (CTLA-4, UC10-4B9), TIM-3 (RMT3-23), CD223 (Lag-3, C9B7W), ICOS (c398.4A), 4-1BB (17B5), GITR (DTA-1), OX-40 (OX-86), PD-L1 (10F.9G2) for *in vivo* studies. Staining signals were acquired on BD LSRFortessa or BD LSR II (BD Biosciences) and analyzed using FlowJo software (FlowJo, LLC).

Cytokine profiling analysis

The supernatant of primed Pmel-1 with or without selumetinib was collected at day 5 after human gp-100 peptide addition and subjected to Luminex cytokine analysis using Luminex MAGPIX system and Milliplex multiplex assays mouse panel (Millipore) and analyzed using xPOTENT software (Millipore Sigma). Mouse lung bronchoalveolar lavage (BAL) from GEMM *KRAS*^{G1C} mice after the treatment was performed by intratracheal injection of 2ml of sterile PBS and collected by aspiration. Cytokines were measured using Mouse Cytokine 23-plex Assay (Bio-Rad) and measured on Bio-Plex 200 system (Bio-Rad). Concentrations [pg/ml] of each protein were derived from 5-parameter curve fitting models. Fold changes relative to the control were calculated and plotted as $\log_2$FC. Lower and upper limits of quantitation (LLOQ/ULOQ) were derived from standard curves for cytokines above or below detection.

Immunohistochemistry (IHC) staining and analyses

Paraffin-embedded sections were deparaffinized, followed by immunohistochemical staining with antibodies against pERK (Cell Signaling) and examined using a Leica upright microscope (Liu et al., 2015b). H&E sections were examined by a pathologist at Dana-Faber Cancer Institute. Results were independently scored by two pathologists using multiplicative quick systems (Liu et al., 2015b). Briefly, the expression score of each marker was calculated by multiplying a score indicating percentage of positively stained cells within tumor cells counted (1 = 0%–4%; 2 = 5%–19%; 3 = 20%–39%; 4 = 40%–59%; 5 = 60%–79%; 6 = 80%–100%) by the intensity grade of staining (0 = negative; 1 = weak; 2 = moderate; 3 = strong).

QUANTIFICATION AND STATISTICAL ANALYSIS

Statistical Analysis

Data are presented as mean with SEM unless otherwise specified. Statistical comparisons were performed using unpaired Student's t tests for two tailed *p* value unless otherwise specified. *$p < 0.05$, **$p < 0.01$, ***$p < 0.001$. Survival was analyzed by Log-rank analysis by Graphad Prism 7.

DATA AND SOFTWARE AVAILABILITY

Data Resources

The accession number for the Affymetrix transcriptome analysis reported in this paper is GEO: GSE126202.

Cell Reports, Volume *27*

Supplemental Information

Pulsatile MEK Inhibition Improves Anti-tumor Immunity and T Cell Function in Murine Kras Mutant Lung Cancer

Hyejin Choi, Jiehui Deng, Shuai Li, Tarik Silk, Lauren Dong, Elliott J. Brea, Sean Houghton, David Redmond, Hong Zhong, Jonathan Boiarsky, Esra A. Akbay, Paul D. Smith, Taha Merghoub, Kwok-Kin Wong, and Jedd D. Wolchok

Figure S1 (Related to Figure 1)

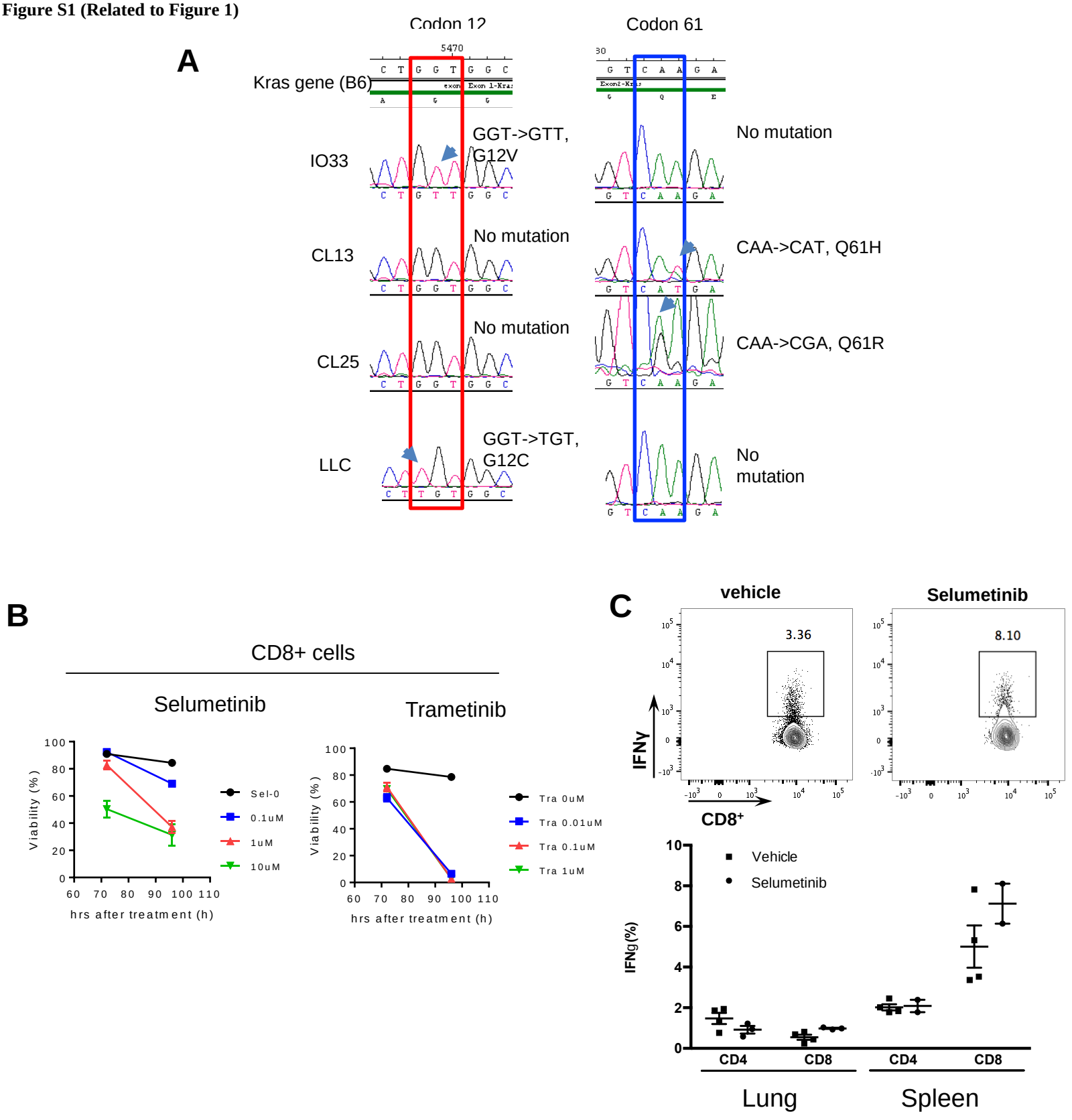

Figure S1. Related to Figure 1. **A.** Kras mutations from diverse murine lung cancer cell lines. Sequencing histogram of codon 12 or codon 61 of Kras gene from IO33, CL13 CL25, and LLC lung cancer cell lines. Red and blue boxes indicate codon 12 and codon 61. Blue arrows indicate changes in a sequence in individual cell lines. **B.** Viability measured by flow cytometry using fixable viability dye after different concentrations of selumetinib (left) or trametinib (right) on splenocytes that were activated with anti-CD3 and anti-CD28 antibodies. **C.** IFNγ expression by flow cytometry of T cells from lung and spleen of tumor-bearing mice (four mice from control group and three mice from treatment group).

Figure S2 (Related to Figure 2)

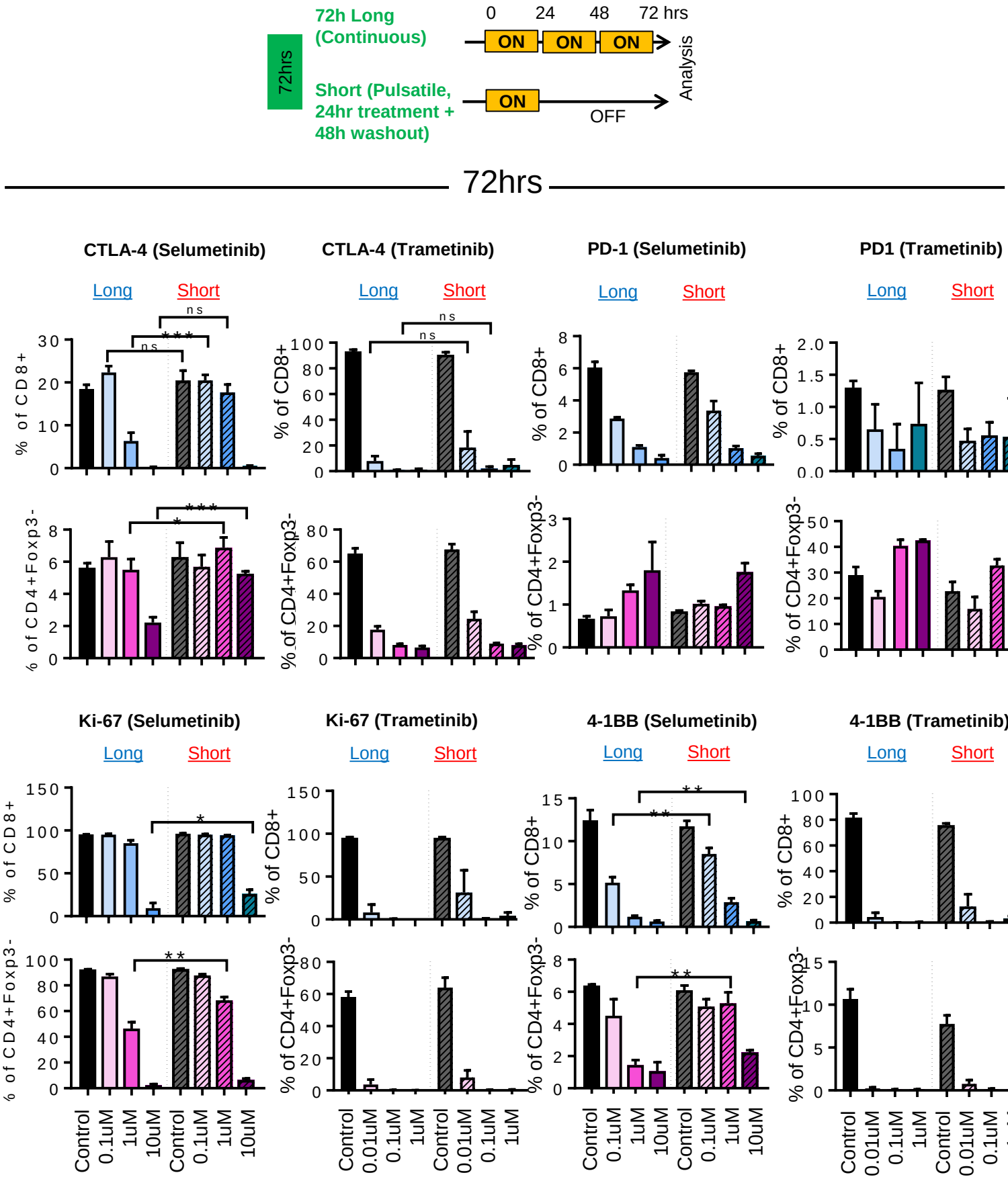

Figure S2. Pulsatile schedule of MEKi treatment altered T cell activation status *in vitro*, Related to Figure 2. CTLA-4, PD1, Ki-67, and 4-1BB expression in CD8+ cells and CD4+Foxp3- cells from spleen of HKP1 lung tumor-bearing mice by flow cytometry after selumetinib (left) and trametinib (right) treatment for 72 hrs. Welch's test, * <0.05, **<0.01, ***<0.001

Figure S3 (Related to Figure 3)

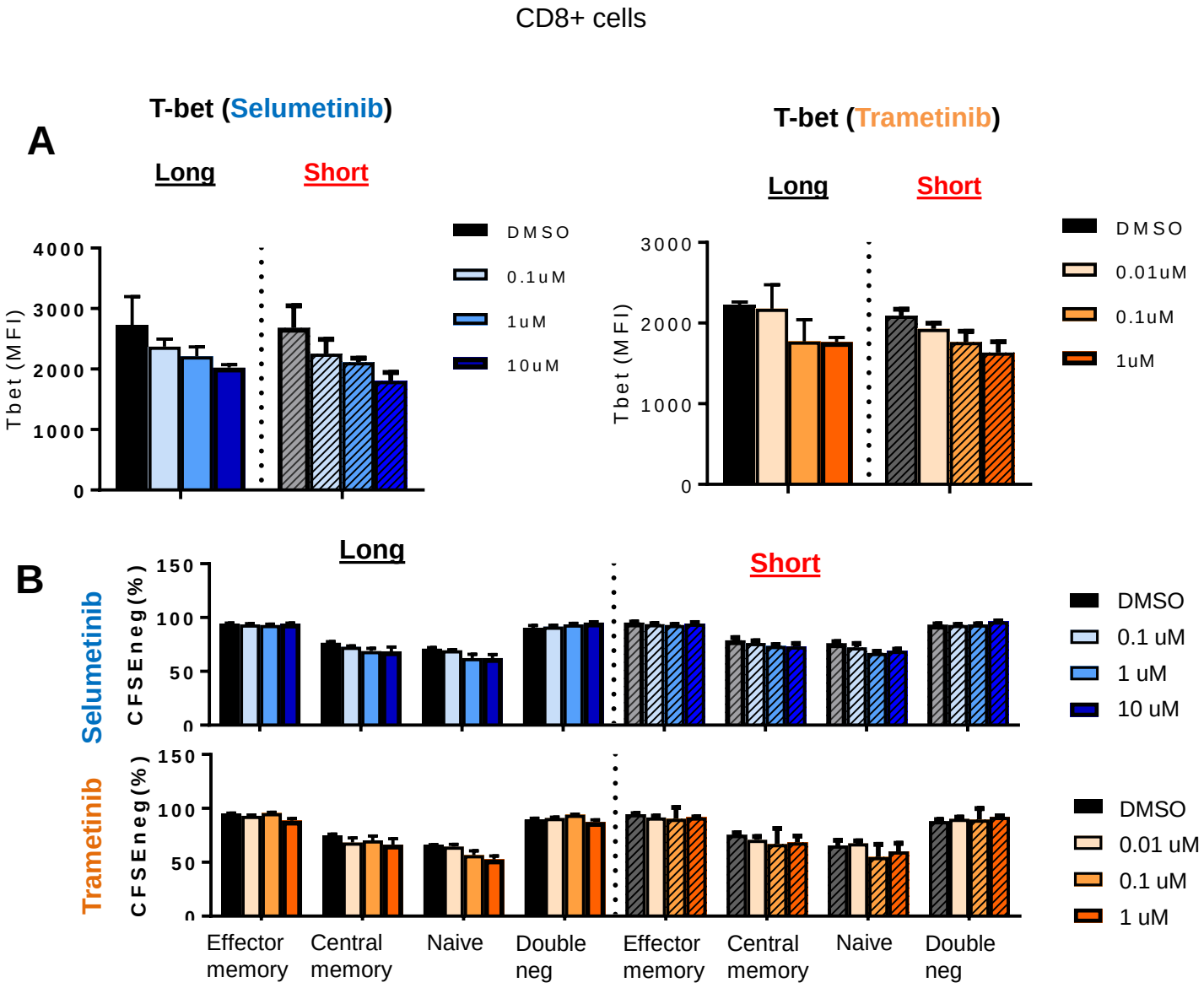

Figure S3. Flow cytometry analysis of primed Pmel-1 CD8+ cells after continuous or pulsatile treatment of MEK inhibitors during priming, Related to Figure 3. **A.** Expression of Tbet from Pmel-1 CD8+ cells after long or short treatment of MEKis by flow cytometry. **B.** Frequency of CFSE negative cells from subsets of CD44 and CD62L combination.

Figure S4 (Related to Figure 4)

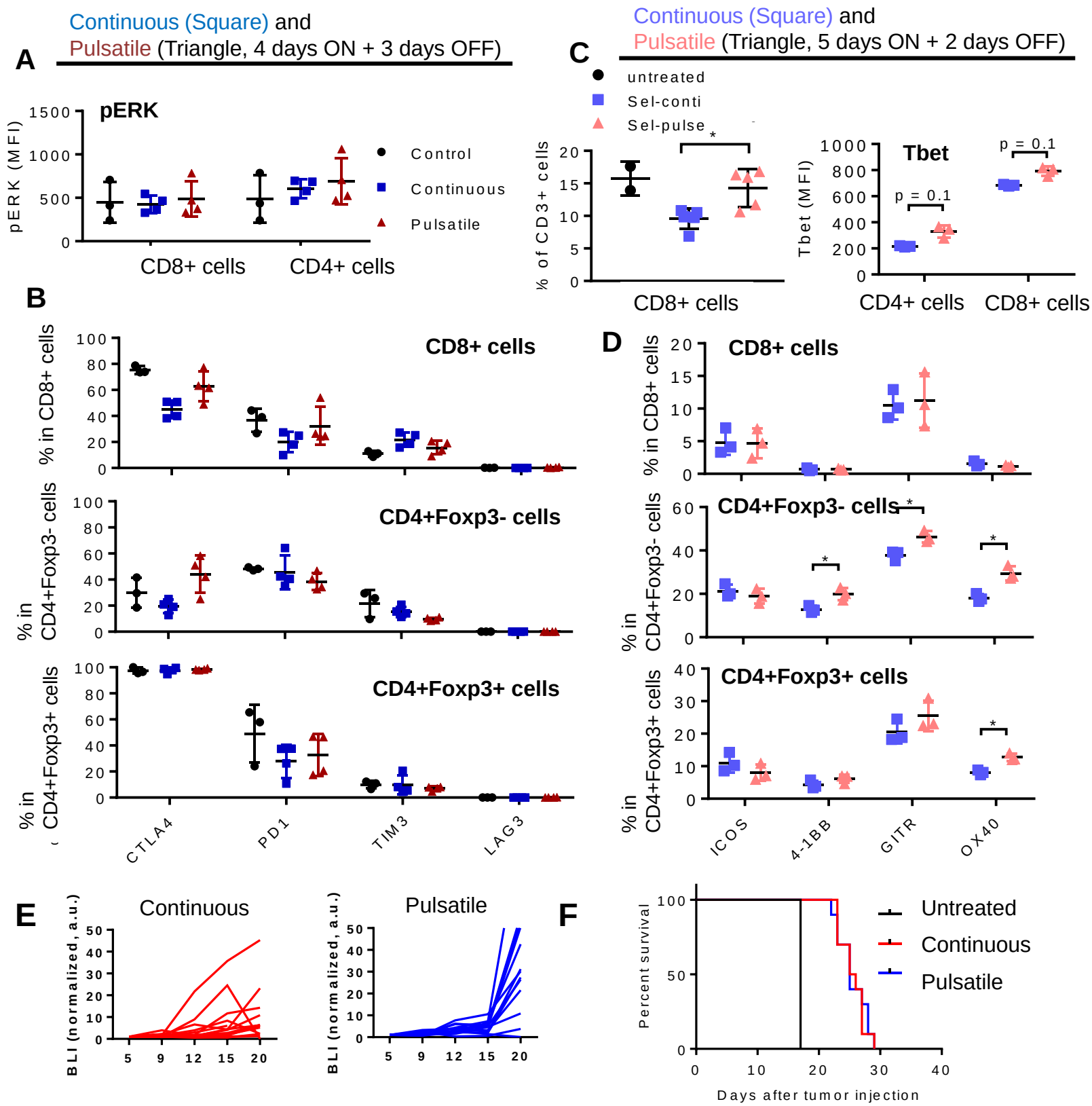

Figure S4. T cells show differential phenotypes with continuous and pulsatile selumetinib treatment, Related to Figure 4. HKP1 lung tumor-bearing mice were treated for 2 weeks either continuously with 25mg/kg of selumetinib twice a day (continuous group) or with pulsatile dosing with 2 cycles of treatment. Pulsatile treatment was done with 300 mg/kg twice a day, 4 days ON and 3 days OFF (Figures A, B) or with 25 mg/kg twice a day, 5 days ON and 2 days OFF (Figures C-F). The control group was treated with vehicle continuously. All mice were sacrificed, and lungs were collected and analyzed by flow cytometry after 2 weeks of treatment. **A.** pERK expression in CD8+ cells and CD4+ cells. **B.** Co-inhibitory markers expression of T cells. **C.** T cell infiltration in tumor lung (left) and Tbet and Eomes expression from T cells in tumor lungs (right). **D.** Co-stimulatory markers expression of T cells in HKP1 tumor lungs. Mann Whitney, * <0.05. **E.** Tumor growth measured by bioluminescence from 5+2 days treatment experiment. **F.** Survival of tumor-bearing mice from 5+2 days treatment.

Figure S5 (Related to Figure 5)

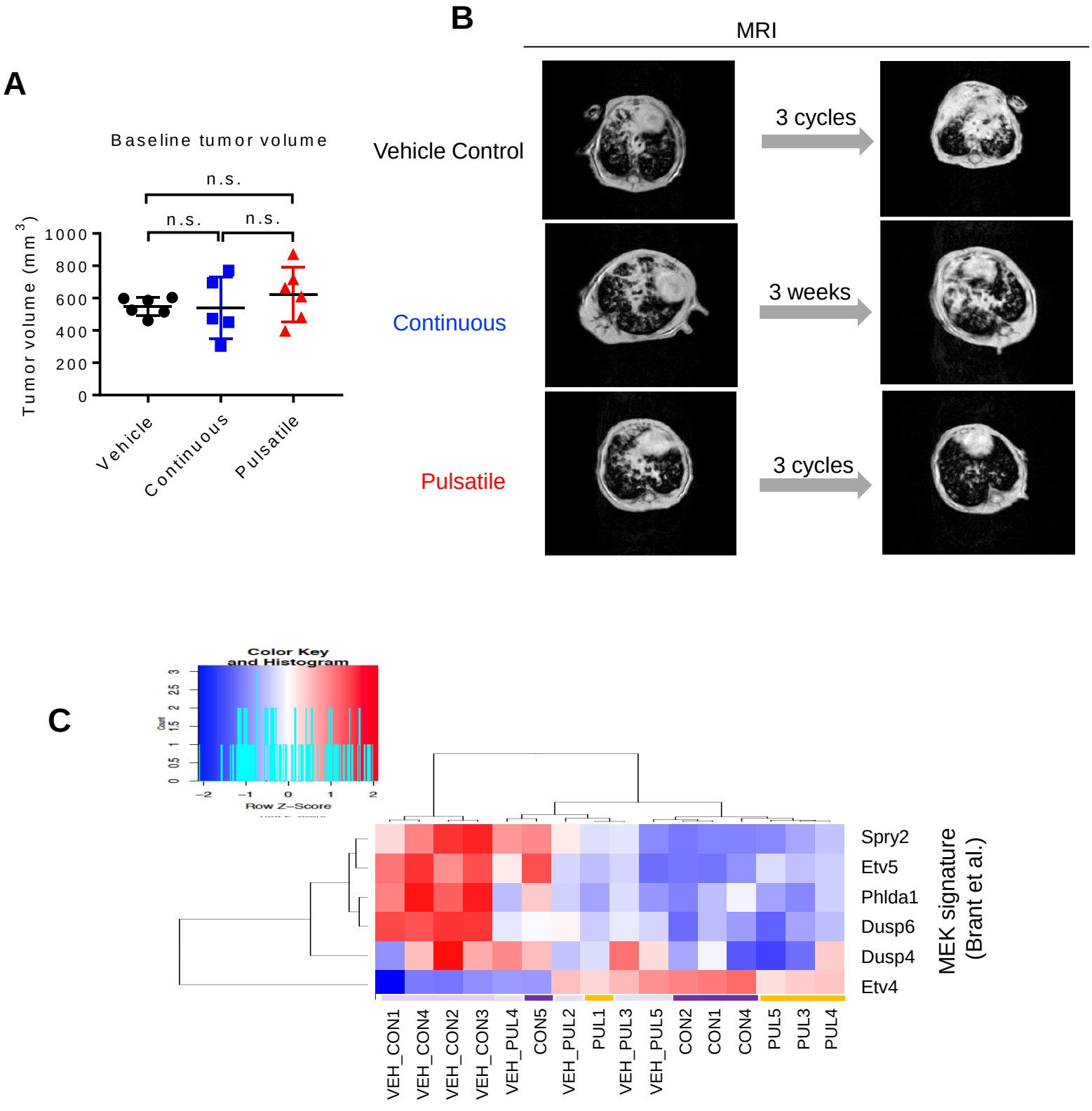

Figure S5. *KRAS*^{G12C} mice treated with pulsatile or continuous selumetinib, Related to Figure 5**. A.** The starting tumor volume of *KRAS*^{G12C} mice with individual treatments at baseline. **B.** Representative images of MRI of ^{KRASG12C} mice before and after treatment with pulsatile selumetinib, continuous selumetinib or vehicle control. **C.** MEK signature from transcriptome analysis of lung tumors. VEH_CON (vehicle for continuous group), CON (continuous group), VEH_PUL (vehicle for pulsatile group), PUL (pulsatile group). Each group has 4 - 5 mice for this analysis.

Figures S6 (Related to Figure 6)

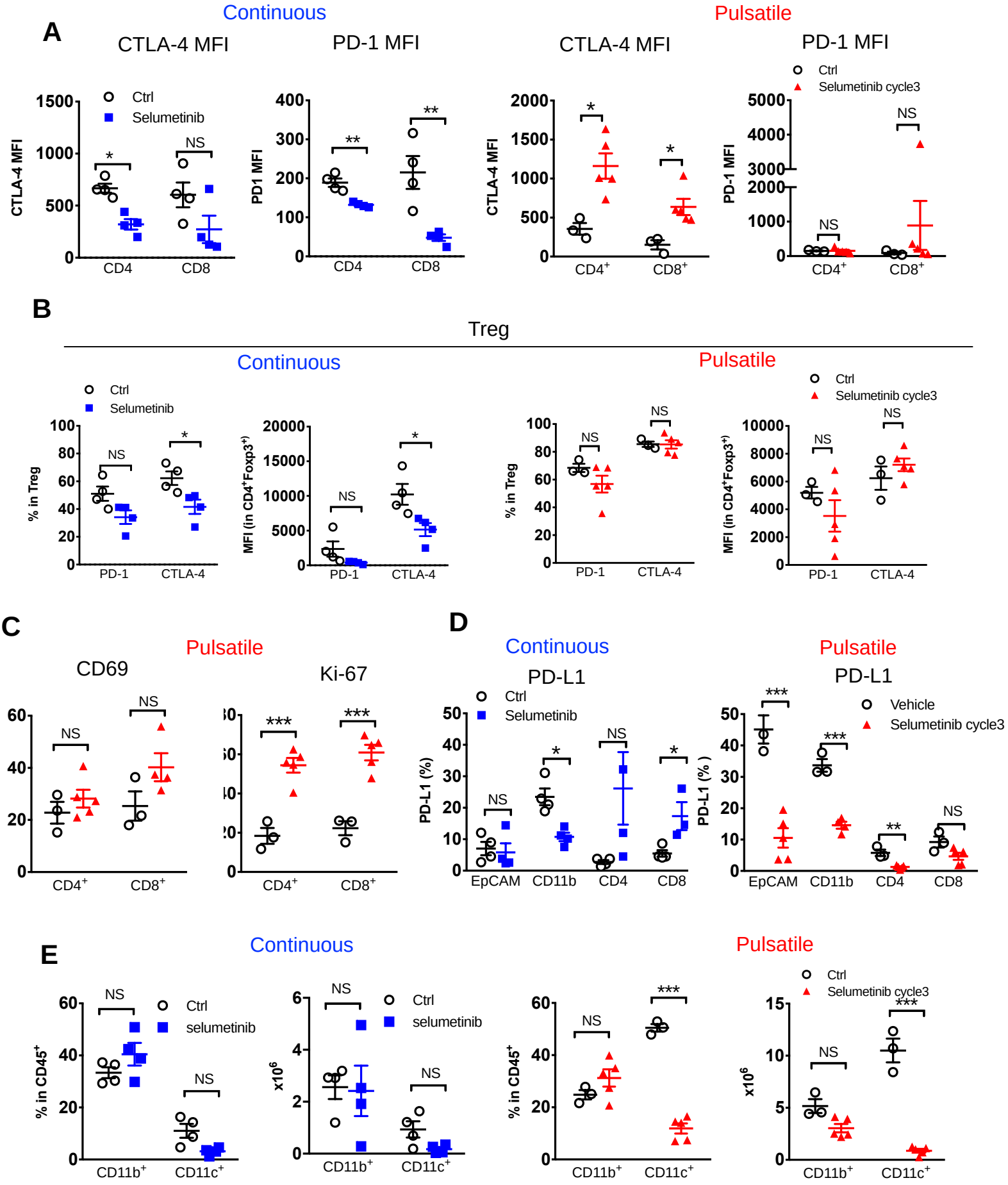

Figure S6. Flow cytometry analysis of selumetinib treated *KRAS*^{G12C} GEMM tumor from Figure 5 experiment, Related to Figure 6. **A.** MFI of CTLA-4 and PD-1 from CD4+ cells and CD8+ cells. **B.** CTLA-4 and PD-1 of Treg cells gated as CD4+Foxp3+ cells. **C.** CD69 and Ki-67 from pulsatile treated mice. **D.** PD-L1 from continuous and pulsatile treatment **E.** Myeloid cells infiltration from continuous and pulsatile treatment. ** < 0.01; *** < 0.001

Figures S7 (Related to Figure 7)

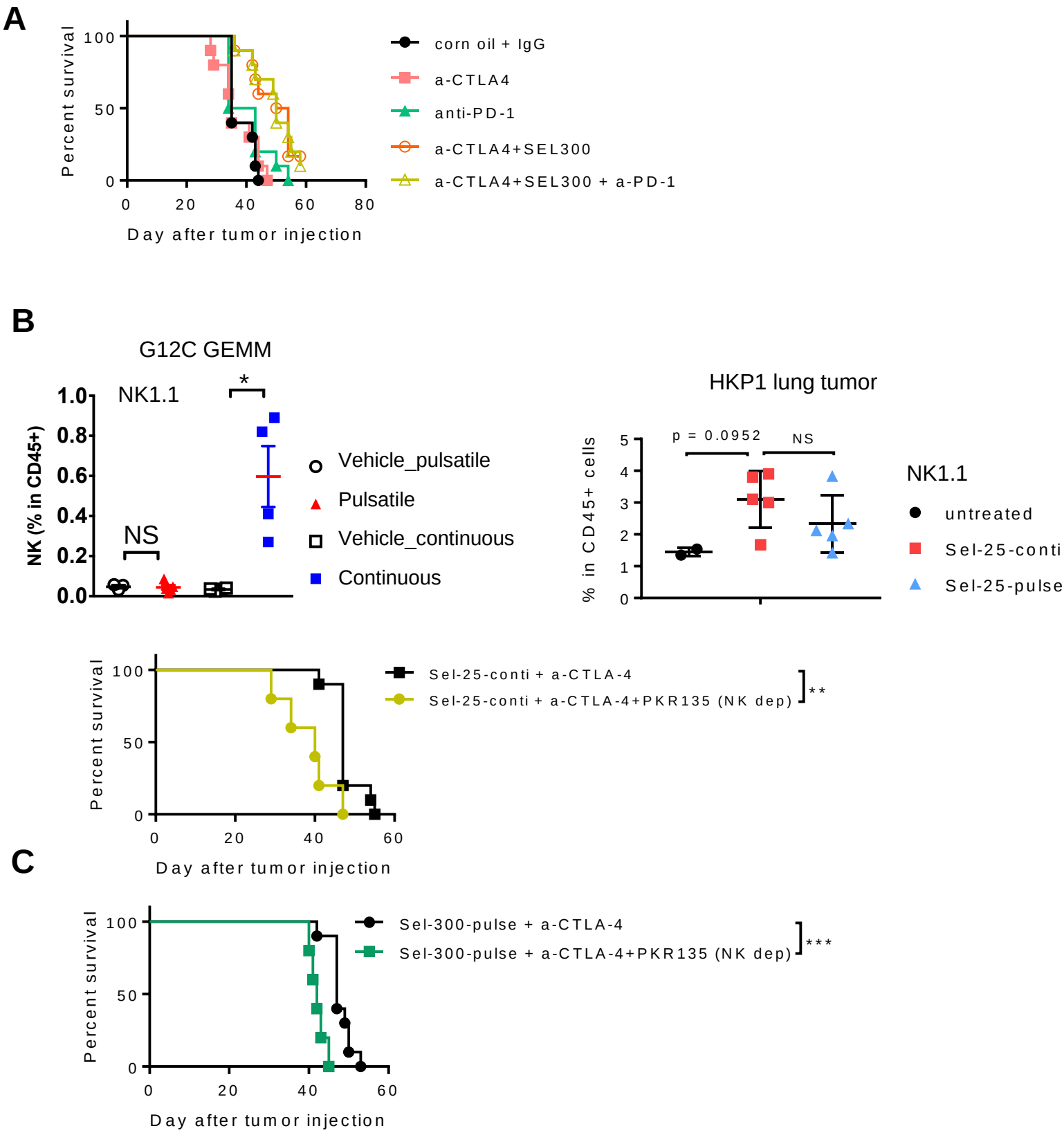

Figure S7. Related to Figure 7. **A.** Survival of anti-PD-1 mono/combination therapy in transplantable LLC model. The experiments were performed twice and representative result was presented. **B.** NK cell infiltration in lung tumors from GEMM and HKP1 transplantable model. **C.** Survival of selumetinib + anti-CTLA-4 treatment with/without NK cells depletion in transplantable LLC model, 4 weeks of treatment. Pulsatile treatment: 4 days ON + 3 days OFF (n = 5). Flow cytometry analysis and survival analysis were performed once. *<0.05; **<0.01; ***<0.001.